

## Nonlocal pair correlations in the one-dimensional Bose gas at finite temperature

— [Source link](#) 

Piotr Deuar, Andrew Sykes, Dimitri M. Gangardt, Matthew J. Davis ...+2 more authors

**Institutions:** University of Paris-Sud, University of Queensland, University of Birmingham, Swinburne University of Technology

**Published on:** 20 Apr 2009 - Physical Review A (American Physical Society)

**Topics:** Bose gas, Ideal gas, Correlation function (statistical mechanics) and Imaginary time

Related papers:

- [Pair Correlations in a Finite-Temperature 1D Bose Gas](#)
- [Exact analysis of an interacting bose gas. i. the general solution and the ground state](#)
- [Thermodynamics of a One-Dimensional System of Bosons with Repulsive Delta-Function Interaction](#)
- [Atomic Scattering in the Presence of an External Confinement and a Gas of Impenetrable Bosons](#)
- [Tonks–Girardeau gas of ultracold atoms in an optical lattice](#)

Share this paper:    

View more about this paper here: <https://typeset.io/papers/nonlocal-pair-correlations-in-the-one-dimensional-bose-gas-1xuij68k0o>

# Nonlocal pair correlations in the one-dimensional Bose gas at finite temperature

P. Deuar,<sup>1,\*</sup> A. G. Sykes,<sup>2</sup> D. M. Gangardt,<sup>3</sup> M. J. Davis,<sup>2</sup> P. D. Drummond,<sup>4</sup> and K. V. Kheruntsyan<sup>2</sup>

<sup>1</sup>Laboratoire Physique Théorique et Modèles Statistique, CNRS, Université Paris-Sud, 91405 Orsay, France

<sup>2</sup>ARC Centre of Excellence for Quantum-Atom Optics, School of Physical Sciences, University of Queensland, Brisbane QLD 4072, Australia

<sup>3</sup>School of Physics and Astronomy, University of Birmingham, Edgbaston, Birmingham B15 2TT, United Kingdom

<sup>4</sup>ARC Centre of Excellence for Quantum-Atom Optics, Centre for Atom Optics and Ultra-fast Spectroscopy, Swinburne University of Technology, Melbourne VIC 3122, Australia

(Received 23 December 2008; published 20 April 2009)

The behavior of the spatial two-particle correlation function is surveyed in detail for a uniform one-dimensional Bose gas with repulsive contact interactions at finite temperatures. Long-, medium-, and short-range effects are investigated. The results span the entire range of physical regimes from ideal gas to strongly interacting and from zero temperature to high temperature (Gross-Pitaevskii) and strongly interacting (Tonks-Girardeau) gases. We present perturbative analytic methods, available at strong and weak couplings, and first-principles numerical results using imaginary time simulations with the gauge- $P$  representation in regimes where perturbative methods are invalid. Nontrivial effects are observed from the interplay of thermally induced bunching behavior versus interaction induced antibunching.

DOI: [10.1103/PhysRevA.79.043619](https://doi.org/10.1103/PhysRevA.79.043619)

PACS number(s): 67.85.Bc, 03.75.Hh, 05.10.Gg, 68.65.-k

## I. INTRODUCTION

The study of two-body correlations has a long history dating back to the 1956 experiment of Hanbury Brown and Twiss (HBT) [1]. The HBT experiment set out to measure the intensity of light coming from a distant star at two nearby points in space. The fluctuations in the intensities were shown to be strongly correlated in spite of the thermal nature of the source. In more recent times, experimental progress in the field of ultracold atomic gases has provided the opportunity to examine similar correlations in systems of cold atoms (as opposed to photonic systems). The large thermal de Broglie wavelength in a cold gas means the correlations occur on length scales large enough to be resolved using current detectors. A pioneering experiment of this kind involving a cloud of cold neon atoms was carried out by Yasuda and Shimizu [2] as early as 1996. A more comprehensive study was undertaken during 2005–2007 in Refs. [3,4], where the two-particle *bunching* phenomena associated with Bose enhancement (when metastable  $^4\text{He}^*$  atoms were used) were juxtaposed with the *antibunching* behavior present in a system of fermions (when  $^3\text{He}^*$  atoms were used). In all of the above cases the measured correlations were completely described by the statistical exchange interaction between particles in an *ideal* gas.

The behavior of strongly *interacting* systems poses some of the most difficult questions confronting current theoretical studies in many-body physics. In this paper we discuss how our simple understanding of two-body correlations in an ideal gas can be radically altered in the presence of interactions. To demonstrate this we calculate the normalized pair correlation function

$$g^{(2)}(r) = \langle \hat{\Psi}^\dagger(0)\hat{\Psi}^\dagger(r)\hat{\Psi}(r)\hat{\Psi}(0) \rangle / n^2 \quad (1)$$

in a homogeneous repulsive one-dimensional (1D) Bose gas [5,6] at finite temperature over a wide range of interaction strengths. In Eq. (1),  $\hat{\Psi}(x)$  is the field operator and  $n = \langle \hat{\Psi}^\dagger(x)\hat{\Psi}(x) \rangle$  is the linear 1D density. Physically,  $g^{(2)}(r)$  quantifies the conditional probability of detecting a particle at position  $r$ , given that a particle has been detected at the origin. Theoretically the 1D Bose gas model with  $\delta$ -function interaction is one of the simplest paradigms we have of a strongly interacting quantum fluid, owing to its exact integrability [5–10]. In the limit of an infinitely strong interaction it corresponds to a gas of impenetrable (hard-core) bosons treated first in Ref. [11]. It also holds relevance as an experimentally accessible system [12–26]. Opposite from two dimensions and three dimensions, the strongly interacting limit of a 1D system is achieved in the low density regime. In this regime the wave function of the particles is strongly correlated and prevents them from being close to each other, which results in dramatic suppression of three-body losses. This allows for the stable creation of strongly interacting 1D Bose gases.

There has been a substantial amount of previous theory on correlations of the 1D Bose gas model. The Luttinger liquid approach provides a method of calculating the long-range asymptotic behavior in the decay of nonlocal correlations [9,10]. Local second- and third-order correlations in the homogeneous system have been calculated in Refs. [27–31]; extensions to inhomogeneous systems using the local density approximation (LDA) are given in Ref. [32]. Numerical calculations at specific values of interaction strength have been carried out at  $T=0$  [33] and at finite temperature [34]. Similar *nonlocal* quantities have been calculated for the  $T=0$  ground state [33,35–41] and for finite temperature both numerically [34] and in the strong interaction limit [42]. References [8–10,43–45] contain recent reviews of the physics of the 1D Bose gas problem.

\*piotr.deuar@lptms.u-psud.fr

The focus of the present paper is the nonlocal correlation function at arbitrary interparticle separations  $r$ ; we give the details of analytic derivations of the results discussed in a recent letter [46] and complement them with exact numerical calculations using the stochastic gauge- $P$  method in Refs. [34,47–50]. Experimental proposals to measure nonlocal spatial correlations between the atoms in a 1D Bose gas have been discussed in Refs. [46,51].

The structure of this paper is as follows. In Sec. II we give a brief review of the physics of a 1D Bose gas, emphasizing the important parameters which determine the phase diagram. In Sec. III we outline the details involved in the application of the (imaginary time) gauge- $P$  phase-space method to the 1D Bose gas. The more technical details are placed in Appendix A. This method is capable of obtaining numerical results in the crossover regions of the phase diagram, where analytic results are not available. In Secs. IV–VI we present the results of calculating  $g^{(2)}(r)$  in the nearly ideal-gas limit, the weakly interacting limit, and the strongly interacting limit, respectively. The results are obtained from numerical calculations and analytic perturbation expansions. We describe the details of our perturbation expansion in each respective section. In Sec. VII we analyze, in detail, the nature of the crossover into the fermionized Tonks gas regime. Section VIII discusses the limitations of the numerical method. In Sec. IX we give an overview and draw conclusions.

## II. INTERACTING BOSE GAS IN ONE DIMENSION

We are considering a homogeneous system of  $N$  identical bosons in a 1D box of length  $L$  with periodic boundary conditions [5,6]. We include two-body interactions in the form of a repulsive delta-function potential. The second-quantized Hamiltonian of the system is given by

$$\hat{H} = \frac{\hbar^2}{2m} \int dx \partial_x \hat{\Psi}^\dagger \partial_x \hat{\Psi} + \frac{g}{2} \int dx \hat{\Psi}^\dagger \hat{\Psi}^\dagger \hat{\Psi} \hat{\Psi}, \quad (2)$$

where  $m$  is the mass and  $g > 0$  is the coupling constant that can be expressed via the three-dimensional (3D)  $s$ -wave scattering length  $a$  as  $g \simeq 2\hbar^2 a / (m l_\perp^2) = 2\hbar \omega_\perp a$  [52]. Here, we have assumed that the atoms are transversely confined by a tight harmonic trap with frequency  $\omega_\perp$  and that  $a$  is much smaller than the transverse harmonic oscillator length  $l_\perp = \sqrt{\hbar / m \omega_\perp}$ . The 1D regime is realized when the transverse excitation energy  $\hbar \omega_\perp$  is much larger than both the thermal energy  $T$  (with  $k_B = 1$ ) and the chemical potential  $\mu$  [32,53]. A uniform system in the thermodynamic limit ( $N, L \rightarrow \infty$ , while the 1D density  $n = N/L$  remains constant) is completely characterized [5,7] by two parameters: the dimensionless interaction strength

$$\gamma = \frac{mg}{\hbar^2 n} \quad (3)$$

and the reduced temperature

$$\tau = T/T_d, \quad (4)$$

where  $T_d = \hbar^2 n^2 / (2m)$  is the temperature of quantum degeneracy in units of energy [30].

The interplay between these two parameters dictates the dominating behavior in six physically different regimes. Briefly, these regimes are:

(i) *Nearly ideal-gas* regime, where the temperature always dominates over the interaction strength. This regime splits into two subregimes defined by  $\tau \ll 1$  or  $\tau \gg 1$ . In both cases one must have  $\gamma \ll \min\{\tau^2, \sqrt{\tau}\}$ .

(ii) *Weakly interacting* regime, where both the interaction strength and the temperature are small, but  $\tau^2 \ll \gamma \ll 1$ . This regime realizes the well-known quasicondensate phase. Fluctuations occur due to either vacuum or thermal fluctuations, which define two further subregimes, with  $\tau \ll \gamma$  or  $\tau \gg \gamma$ , respectively.

(iii) *Strongly interacting* regime, where the interaction strength is large and dominates over temperature induced effects. This can occur at high and low temperatures, again defining two subregimes with  $\tau \ll 1$  or  $\tau \gg 1$ .

The basic understanding of the competition between interaction induced effects and thermally induced effects was outlined in Ref. [46].

Although the model is integrable via the Bethe ansatz, the cumbersome nature of the eigenstates [54] inhibits the direct calculation of the nonlocal two-body correlation function. We therefore use numerical integration in a phase-space representation, together with perturbation theory in each of the six regimes. The standard Bogoliubov procedure, applied to Eq. (2), is appropriate in the case of the weakly interacting regime (see Sec. V). Perturbation theory in the strongly interacting and nearly ideal-gas regimes is done using the path integral formalism (see Secs. IV A and VI, respectively).

## III. NUMERICAL STOCHASTIC GAUGE CALCULATIONS

### A. Gauge- $P$ distribution

To evaluate correlations away from the regimes of applicability of the analytic approximations, we use the gauge- $P$  phase-space method to generate a stochastic evolution from the simple  $T \rightarrow \infty$  limit (where interactions are negligible) down to lower temperatures. This method gives results that correspond exactly to the full quantum mechanics using Hamiltonian (2) as the number of averaged realizations ( $\mathcal{S}$ ) goes to infinity. The gauge- $P$  method has been described in [47–49] and is covered in greatest detail in [50], while an initial application to the 1D Bose gas was presented in [34]. Below we give a summary of the derivation for this system and present the basic calculation procedure. Some of the more technical details are given in Appendix A.

We consider a grand canonical ensemble with mean density  $n$ , Hamiltonian (2), and inverse temperature given by  $\beta = 1/k_B T$ . When the Hamiltonian commutes with the number operator  $\hat{N} = \int dx \hat{\Psi}^\dagger(x) \hat{\Psi}(x)$ , as is the case here, the unnormalized density matrix at temperature  $T$  is given by

$$\hat{\rho}_u = e^{[\mu(\beta)\hat{N} - \hat{H}]\beta}, \quad (5)$$

where  $\mu(\beta)$  is the chemical potential. In this formulation,  $\mu$  can, in principle, be chosen at will as any desired function of temperature, thus indirectly determining the density  $n(T)$ . In

the Schrödinger picture the density matrix is equivalently defined by an “imaginary time” masterlike equation

$$\frac{\partial \hat{\rho}_u(\beta)}{\partial \beta} = [\mu_e(\beta) \hat{N} - \hat{H}] \hat{\rho}_u(\beta) = \frac{1}{2} [\mu_e(\beta) \hat{N} - \hat{H}, \hat{\rho}_u(\beta)]_+ \quad (6)$$

and a simple initial (i.e.,  $T \rightarrow \infty$ ) condition

$$\hat{\rho}_u(0) = e^{-\lambda \hat{N}}, \quad (7)$$

with  $\lambda = -\lim_{\beta \rightarrow 0} [\beta \mu(\beta)]$  and  $\beta$  playing a similar role to time in the Schrodinger equation for time evolution, apart from a factor of  $i$  (hence the name). The second part of Eq. (6) follows from the restricted set of density matrices described by the grand canonical ensemble (5), where  $\log \hat{\rho}_u$  commutes with  $\hat{\rho}_u$ . Note that  $\mu_e(\beta)$  is a temperature-dependent “effective” chemical potential,

$$\mu_e = \frac{\partial [\beta \mu(\beta)]}{\partial \beta}, \quad (8)$$

which is not necessarily equal to  $\mu$ . The initial condition (7) can then be evolved according to Eq. (6) to obtain the equilibrium state at lower temperatures  $\beta > 0$ . However, in the density matrix form, this naturally becomes intractable for more than a few particles.

Phase-space methods such as the gauge- $P$  distribution used here reduce the computational resources needed to a manageable number. This is done by deriving a Fokker-Planck equation (FPE) for a distribution of phase-space variables that is equivalent to the full quantum mechanics (6) and, then in a second step, sampling this distribution stochastically and evolving the *samples* with a diffusive random walk that is equivalent to the Fokker-Planck equation. The general approach is described in [55,56]. The price that is paid for tractable calculations is a loss of precision that comes about due to the finite sample size  $\mathcal{S}$ . Fortunately this uncertainty can be readily estimated using the central limit theorem and scales as  $\sqrt{\mathcal{S}}$ .

We utilize the normalized off-diagonal coherent state expansion of the positive- $P$  distribution [55] because the number of variables required to describe a sample is linear in the number of spatial points (tractability) and because it describes all quantum states with a non-negative real distribution. However, for this investigation two additional elements are needed. First, evolution (6) does not preserve the trace, so an additional weight variable in the expansion is needed to keep track of this. Second, the evolution equations for the samples given by a bare weighted positive- $P$  treatment are unstable and can lead to systematically bad sampling [57]. The complex part of the weight variable allows us to remove these instabilities using a stochastic gauge as described in [34,47].

In practice, the first step is to discretize space into  $M$  equally spaced points in a box of length  $L$  with periodic boundary conditions, on which the fields are defined. There is a lattice spacing of  $\Delta x = L/M$  per point. One must make sure that the lattice is fine enough and long enough to encompass all relevant detail. In practice we check this by increasing  $L$  and, separately,  $M$  until no further change in the

results is seen. Having this equivalent lattice, one can expand the density matrix  $\hat{\rho}_u$  as

$$\hat{\rho}_u = \int G(\vec{v}) \hat{\Lambda}(\vec{v}) d^{4M+2} \vec{v}, \quad (9)$$

with a positive [47] distribution  $G(\vec{v})$  of the set of  $2M+1$  complex phase-space variables,

$$\vec{v} = \{\alpha_1, \dots, \alpha_M, \alpha_1^+, \dots, \alpha_M^+, \Omega\}, \quad (10)$$

which describe an operator basis

$$\hat{\Lambda}(\vec{v}) = \Omega \otimes_{j=1}^M ||\alpha_j\rangle \langle \alpha_j^+|^* || \exp\left(-\sum_{j=1}^M \alpha_j^+ \alpha_j\right), \quad (11)$$

composed of un-normalized (Bargmann) coherent states  $||\alpha_j\rangle = \exp[\alpha_j \sqrt{\Delta x} \hat{\Psi}^\dagger(x_j)] |0\rangle$  at the  $j$ th point at location  $x_j = (j-1)\Delta x$  and a global weight  $\Omega$ .

The initial condition (7) corresponds to the distribution

$$G_0(\vec{v}) = \delta^2(\Omega - 1) \prod_{j=1}^M \delta^2[\alpha_j - (\alpha_j^+)^*] \frac{\exp(-|\alpha_j|^2/\bar{n}_x)}{\pi \bar{n}_x}, \quad (12)$$

where  $\bar{n}_x = 1/(e^\lambda - 1) = N/M$  is the mean number of atoms ( $N = \langle \hat{N} \rangle$ ) per spatial point in the initial  $\beta=0$  state. We see that, at least initially,  $\alpha^+ = (\alpha)^*$  are complex conjugates.

## B. Fokker-Planck equation

To generate the FPE for  $G(\vec{v})$  corresponding to the master equation [Eq. (6)] we use the following differential identities for the basis operators:

$$\sqrt{\Delta x} \hat{\Psi}(x_j) \hat{\Lambda} = \alpha_j \hat{\Lambda}, \quad (13a)$$

$$\sqrt{\Delta x} \hat{\Psi}^\dagger(x_j) \hat{\Lambda} = \left( \alpha_j^+ + \frac{\partial}{\partial \alpha_j} \right) \hat{\Lambda}, \quad (13b)$$

$$\sqrt{\Delta x} \hat{\Lambda} \hat{\Psi}(x_j) = \alpha_j^+ \hat{\Lambda}, \quad (13c)$$

$$\sqrt{\Delta x} \hat{\Lambda} \hat{\Psi}^\dagger(x_j) = \left( \alpha_j + \frac{\partial}{\partial \alpha_j^+} \right) \hat{\Lambda}. \quad (13d)$$

These convert quantities involving the operators  $\hat{\Psi}$ ,  $\hat{\Psi}^\dagger$ , and  $\hat{\rho}_u$  to ones involving only  $\hat{\Lambda}$  and their derivatives.

In what follows it will be convenient to label the  $\alpha$  and  $\alpha^+$  variables as

$$\alpha_j^{(\nu)} = \begin{cases} \alpha_j & \text{if } \nu = 1 \\ \alpha_j^+ & \text{if } \nu = 2. \end{cases}$$

Using Eq. (13) on Eq. (6) one obtains

$$\int \frac{\partial G(\vec{v})}{\partial \beta} \hat{\Lambda} d^{4M+2}\vec{v} = - \int G(\vec{v}) \left\{ \frac{g}{4\Delta x} \sum_{j,v} (\alpha_j^{(v)})^2 \frac{\partial^2}{\partial (\alpha_j^{(v)})^2} + K(\vec{v}) + \frac{1}{2} \sum_j \left[ \left( \frac{\partial K(\vec{v})}{\partial \alpha_j^+} \right) \frac{\partial}{\partial \alpha_j} + \left( \frac{\partial K(\vec{v})}{\partial \alpha_j} \right) \frac{\partial}{\partial \alpha_j^+} \right] \right\} \hat{\Lambda} d^{4M+2}\vec{v}, \quad (14)$$

with

$$N_j = \alpha_j^+ \alpha_j, \quad (15)$$

which is initially the number of particles at the  $j$ th site and an effective complex-variable Gibbs factor  $K$  corresponding to  $\text{Tr}[(\hat{H} - \mu_e \hat{N}) \hat{\Lambda}] / \text{Tr}[\hat{\Lambda}]$ ,

$$K(\vec{v}) = \sum_j \left\{ \frac{\hbar^2 (\nabla \alpha_j^+) (\nabla \alpha_j)}{2m} - \mu_e N_j + \frac{g N_j^2}{2\Delta x} \right\}. \quad (16)$$

Here  $\nabla \alpha_j$  is the discretized analog of the gradient of a complex field  $\alpha(x)$  that satisfies  $\alpha(x_j) = \alpha_j$ .

To obtain a FPE equation for  $G(\vec{v})$  we proceed as follows. First, we can make use of the additional ‘‘gauge’’ identity that follows trivially from Eq. (11),

$$\left( \Omega \frac{\partial}{\partial \Omega} - 1 \right) \hat{\Lambda} = 0, \quad (17)$$

to convert  $K(\vec{v}) \hat{\Lambda} = K(\vec{v}) \Omega \frac{\partial}{\partial \Omega} \hat{\Lambda}$  on the first line of Eq. (14). This step is necessary in order to obtain an equation of a form that can later be sampled with a diffusive process. Second, we integrate by parts to obtain differentials of  $G$  rather than  $\hat{\Lambda}$ . Third, if the distribution  $G$  is well bounded as  $|\alpha_j|, |\alpha_j^+|, |\Omega| \rightarrow \infty$ , we can discard the boundary terms. As it turns out (see Appendix A 1), this is not fully justified for the Eq. (14), and the boundary behavior will need to be improved with the help of a stochastic gauge as described originally in [47]. However, for demonstrative purposes let us proceed for now and return to the remedy of the problem below in Sec. III D. Lastly, having now an equation of the form  $\int \hat{\Lambda} \times [\text{differential operator}] G(\vec{v}) d\vec{v} = 0$ , one solution is certainly  $[\text{differential operator}] G(\vec{v}) = 0$ , which is the following FPE:

$$0 = - \left\{ \frac{\partial}{\partial \Omega} \Omega K(\vec{v}) - \frac{\partial}{\partial \beta} \sum_{j,v} \left[ \frac{g}{4\Delta x} \frac{\partial^2}{\partial (\alpha_j^{(v)})^2} (\alpha_j^{(v)})^2 + \frac{1}{2} \frac{\partial}{\partial \alpha_j^{(v)}} \left( \frac{\hbar^2 (\nabla^2 \alpha_j^{(v)})}{2m} + \mu_e \alpha_j^{(v)} - \frac{g \alpha_j^{(v)} N_j}{\Delta x} \right) \right] \right\} G(\vec{v}). \quad (18)$$

### C. Equivalent diffusion

A diffusive random walk that corresponds to the Fokker-Planck equation [Eq. (18)] is found by replacing the analytic derivatives with appropriate derivatives of the real and imaginary parts of  $\alpha_j^{(v)}$  [55,56]. This results in a diffusion matrix in the phase-space variables  $\vec{v}$  with no negative eigen-

values. In the Ito calculus this is equivalent to the following set of stochastic differential equations:

$$\frac{d\alpha_j^{(v)}}{d\beta} = \frac{1}{2} \left( \mu_e + \frac{\hbar^2 \nabla^2}{2m} - \frac{g N_j}{\Delta x} \right) \alpha_j^{(v)} + i \alpha_j^{(v)} \sqrt{\frac{g}{2\Delta x}} \zeta_j^{(v)}(\beta), \quad (19)$$

$$\frac{d\Omega}{d\beta} = -\Omega K(\vec{v}).$$

We do not use diffusion gauges [49] here and decompose the diffusion matrix in the most straightforward fashion. Here, the  $\zeta_j^{(v)}(\beta)$  are real, delta-correlated, independent white Gaussian noise fields that satisfy the stochastic averages,

$$\langle \zeta_j^{(v)}(\beta) \rangle_S = 0, \quad (20a)$$

$$\langle \zeta_i^{(v)}(\beta) \zeta_j^{(v')}(\beta') \rangle_S = \delta_{ij} \delta_{vv'} \delta(\beta - \beta'). \quad (20b)$$

In practice, at each time step separated from the subsequent by an interval  $\Delta\beta$ , one generates  $M$  independent real Gaussian random variables of variance  $1/\Delta\beta$  for each  $\zeta_j^{(v)}$ .

Equations (19) can be intuitively interpreted by noting that the equation for the amplitudes  $\alpha_j^{(v)}$  at each point is a Gross-Pitaevskii equation in imaginary time, with some extra noises that emulate the wandering of trajectories in a path integral formulation around the mean field solution given by the deterministic part. The weight evolution of  $\Omega$  generates the Gibbs factors of the grand canonical ensemble.

### D. Final equations

A straightforward application of the diffusion equations [Eq. (19)] is foiled by the presence of an instability in the  $d\alpha_j^{(v)}/d\beta$  equations. We use a stochastic gauge to remove this instability, in a manner described in [49,50], with the details given in Appendix A 1. The final Ito stochastic equations of the samples are

$$\frac{d\alpha_j^{(v)}}{d\beta} = \frac{1}{2} \left[ \mu_e + \frac{\hbar^2 \nabla^2}{2m} - \left( \frac{g}{\Delta x} \right) (|N_j| - i \text{Im } N_j) + i \zeta_j^{(v)}(\beta) \sqrt{\frac{2g}{\Delta x}} \right] \alpha_j^{(v)},$$

$$\frac{d\Omega}{d\beta} = \Omega \left[ -K(\vec{v}) - i \sqrt{\frac{g}{2\Delta x}} \sum_{j,v} \zeta_j^{(v)}(\beta) (|N_j| - \text{Re } N_j) \right]. \quad (21)$$

Some technical details regarding integration procedure, importance sampling, and choice of  $\mu_e(\beta)$  are given in Appendix A. Attention to these issues can speed up the calculations and reduce sampling errors by orders of magnitude.

### E. Evaluating observables

Given  $\mathcal{S}$  realizations of the variable sets  $\vec{v}$ , using fresh initial samples and noises  $\zeta_j^{(v)}(\beta)$  each time, one generates an estimate of the expectation value of an observable  $\hat{O}$  as follows:



$$\begin{aligned}
E[\hat{O}] &= \frac{\text{Tr}[\hat{O}\hat{\rho}_u]}{\text{Tr}[\hat{\rho}_u]} = \frac{\int G(\vec{v})\text{Tr}[\hat{O}\hat{\Lambda}(\vec{v})]d\vec{v}}{\int G(\vec{v})\text{Tr}[\hat{\Lambda}(\vec{v})]d\vec{v}} \\
&= \frac{\langle \text{Tr}[\hat{O}\hat{\Lambda}(\vec{v})] \rangle_S}{\langle \text{Tr}[\hat{\Lambda}(\vec{v})] \rangle_S} \\
&= \frac{\text{Re}\langle \mathcal{F}[\hat{O}, \vec{v}] \rangle_S}{\text{Re}\langle \Omega \rangle_S}, \quad (22)
\end{aligned}$$

where  $\langle \cdots \rangle_S$  denotes a stochastic average over the samples and  $\mathcal{F}$  is an appropriate function of the phase-space variables  $\vec{v}$ . The last line follows from properties of the operator basis  $\hat{\Lambda}$  and because the traces of  $\hat{\rho}_u$  and of expectation values are real.

Identities [Eq. (13)] can be used to readily evaluate  $\mathcal{F}$  since  $\text{Tr}[\hat{\Lambda}] = \Omega$ . In particular,

$$\langle \hat{\Psi}^\dagger(x_j)\hat{\Psi}(x_j) \rangle = \frac{\text{Re}\langle (N_j\Omega) \rangle_S}{\Delta x \text{Re}\langle \Omega \rangle_S}, \quad (23)$$

$$\langle \hat{\Psi}^\dagger(x_i)\hat{\Psi}^\dagger(x_j)\hat{\Psi}(x_j)\hat{\Psi}(x_i) \rangle = \frac{\text{Re}\langle (N_i N_j \Omega) \rangle_S}{(\Delta x)^2 \text{Re}\langle \Omega \rangle_S}, \quad (24)$$

which explains the relationship between  $N_j$  and the particle number at the  $j$ th site. For the uniform system considered here, it is efficient to average the quantities over the entire lattice, so that, e.g.,

$$g^{(2)}(r) = \frac{L \left\langle \int \hat{\Psi}^\dagger(x)\hat{\Psi}^\dagger(x+r)\hat{\Psi}(x+r)\hat{\Psi}(x)dx \right\rangle}{\left\langle \int \hat{\Psi}^\dagger(x)\hat{\Psi}(x)dx \right\rangle^2}. \quad (25)$$

Uncertainty is estimated as follows: we separate the  $\mathcal{S}$  realizations into  $\mathcal{B}$  bins, such that  $\mathcal{B} \gg 1$  and  $\mathcal{S}/\mathcal{B} \gg 1$ . One calculates an estimate for the expectation value of an observable in each bin independently (let us denote  $\bar{O}_i$  as the estimate obtained from the  $i$ th bin). The best estimate for the expectation value of the observable is obviously  $\langle \bar{O} \rangle_B$ . The one-sigma uncertainty in this estimate is obtained from the central limit theorem and is

$$\Delta \bar{O} = \sqrt{\frac{\langle \bar{O}^2 \rangle_B - \langle \bar{O} \rangle_B^2}{\mathcal{B}}}. \quad (26)$$

#### IV. NEARLY IDEAL GAS REGIME [ $\gamma \ll \min\{\tau^2, \sqrt{\tau}\}$ ]

We now present the perturbation theory results for the decoherent regime of a 1D Bose gas [30], where both the density and phase fluctuations are large and the local pair correlation  $g^{(2)}(0)$  is always close to the result for noninteracting bosons,  $g^{(2)}(0) = 2$ . Depending on the value of the temperature parameter  $\tau$ , we further distinguish two subregimes:

decoherent classical (DC) regime for  $\tau \gg 1$  and decoherent quantum (DQ) regime for temperatures well below quantum degeneracy,  $\tau \ll 1$ . Both can be treated using perturbation theory with respect to the coupling constant  $g$  around the ideal Bose gas, for which the nonlocal pair correlation function has been studied in Ref. [24]. Here, we extend these results to account for the first-order perturbative terms.

#### A. Perturbation theory in $\gamma$

The correlations of a 1D Bose gas are governed by the action

$$S[\Psi^*\Psi] = \int_0^\beta d\sigma \int dr [\Psi^* \partial_\sigma \Psi - \mathcal{H}(\Psi^*, \Psi)], \quad (27)$$

written in terms of a space and imaginary time-dependent  $c$ -number fields  $\Psi(x, \sigma)$  in the Feynman path integral formalism. Here  $\sigma$  is the imaginary time and  $\beta = 1/k_B T$  is the maximum, corresponding to the inverse temperature. The Hamiltonian density  $\mathcal{H}$  is obtained from Eq. (2) by replacing the operators with the  $c$ -number fields. Using action (27), the pair correlation function is given by

$$g^{(2)}(r) = \frac{1}{n^2 Z} \int \mathcal{D}\Psi^*\Psi e^{-S[\Psi^*\Psi]} \Psi^*(0)\Psi^*(r)\Psi(r)\Psi(0), \quad (28)$$

where  $Z = \int \mathcal{D}\Psi^*\Psi e^{-S[\Psi^*\Psi]}$  is the partition function. In Eq. (28) and below, we use the notation that fields with imaginary time dependence omitted act at  $\sigma = 0$ , i.e.,  $\Psi(r) \equiv \Psi(r, 0)$ . Expanding action (27) in powers of  $g$ , we obtain up to the first order,

$$\begin{aligned}
g^{(2)}(r) &= g_{\text{ideal}}^{(2)}(r) - \frac{g}{2n^2} \int_0^\beta d\sigma \int dr' \langle \Psi^*(r', \sigma)\Psi^*(r', \sigma) \\
&\quad \times \Psi(r', \sigma)\Psi(r', \sigma)\Psi^*(0)\Psi^*(r)\Psi(r)\Psi(0) \rangle, \quad (29)
\end{aligned}$$

where  $g_{\text{ideal}}^{(2)}(r) = 1 + G(r, 0^-)G(-r, 0^-)/n^2$  is the ideal Bose gas result following from Wick's theorem. Note that since the expansion above is formally in powers of  $g$ , the final result can always be expressed in powers of  $\gamma$  as  $\gamma^\alpha g$ . The average in Eq. (29) is evaluated using Wick's theorem [58],

$$\begin{aligned}
\Delta g^{(2)}(r) &= g^{(2)}(r) - g_{\text{ideal}}^{(2)}(r) \\
&= -\frac{2g}{n^2} \int_0^\beta d\sigma \int dr' \times G(r', \sigma)G(r-r', -\sigma) \\
&\quad \times G(r'-r, \sigma)G(-r', -\sigma), \quad (30)
\end{aligned}$$

with the Green's function

$$G(r, \sigma) = -\langle \Psi(0, 0)\Psi^*(r, \sigma) \rangle = \frac{1}{\beta L} \sum_{k, n} \frac{e^{ikr - i\hbar\omega_n \sigma}}{i\hbar\omega_n - \hbar^2 k^2/2m + \mu}. \quad (31)$$

The  $\omega_n(\beta)$  are the Matsubara frequencies and the imaginary time  $\sigma$  runs between 0 and  $\beta$ . The Green's function is periodic in the case of bosons and antiperiodic in the case of fermions. Thus it can be Fourier transformed with  $\omega_n$

$=2\pi n/\beta$  (bosons) or  $\omega_n=\pi(2n+1)/\beta$  (fermions). The discrete sum over  $k$  becomes an integral in thermodynamic limit.

In terms of a Green's function  $G_k(\sigma)$  that is Fourier transformed with respect to the spatial coordinates,  $\Delta g^{(2)}(r)$  can be brought to the form

$$\Delta g^{(2)}(r) = -\frac{2g}{n^2} \int_0^\beta d\sigma \int \frac{dk}{2\pi} e^{ikr} \Gamma(k, \sigma) \Gamma(k, -\sigma), \quad (32)$$

where

$$\Gamma(k, \sigma) = \frac{1}{2\pi} \int dp G_{p+k}(\sigma) G_p(-\sigma) \quad (33)$$

and

$$G_k(\sigma) = \begin{cases} -n_k(\beta) e^{-\sigma(\hbar^2 k^2/2m - \mu)}, & \sigma < 0 \\ -[1 + n_k(\beta)] e^{-\sigma(\hbar^2 k^2/2m - \mu)}, & \sigma > 0, \end{cases} \quad (34)$$

with

$$n_k(\beta) = \frac{1}{e^{(\hbar^2 k^2/2m - \mu)\beta} - 1} \quad (35)$$

being the standard bosonic occupation numbers.

### B. Decoherent classical regime

For temperatures above quantum degeneracy,  $\tau \gg 1$ , the chemical potential is large and negative, so the bosonic occupation numbers are small,  $n_k(\beta) \ll 1$ , and can be approximated by the Boltzmann distribution,  $n_k(\beta) \approx e^{-(\hbar^2 k^2/2m - \mu)\beta}$ . Accordingly, the function  $G_k(\sigma)$  in Eq. (34) becomes a Gaussian,

$$G_k(\sigma) = \begin{cases} -\exp[-(\hbar^2 k^2/2m - \mu)(\sigma + \beta)], & \sigma < 0 \\ -\exp[-(\hbar^2 k^2/2m - \mu)\sigma], & \sigma > 0 \end{cases} \quad (36)$$

and Eq. (33) is integrated to yield

$$\Gamma(k, \sigma) = \Gamma(k, -\sigma) = n e^{-\sigma(\beta - \sigma)\hbar^2 k^2/2m\beta}. \quad (37)$$

Here the mean density at a given temperature and chemical potential is determined from  $n = \frac{1}{2\pi} \int dk G_k(0^-) = \sqrt{m/(2\pi\hbar^2\beta)} e^{\beta\mu}$ . Using Eq. (37), the correction (32) to the pair correlation function is found as (see Appendix B)

$$\Delta g^{(2)}(r) = -\gamma \sqrt{\frac{2\pi}{\tau}} \operatorname{erfc}\left(\sqrt{\frac{\pi^2 r^2}{2}}\right), \quad (38)$$

where  $\operatorname{erfc}(x)$  is the complimentary error function.

Together with  $g_{\text{ideal}}^{(2)}(r) = 1 + \exp[-\pi^2 r^2/2]$  ( $\tau \gg 1$ ), this gives the following result for the pair correlation function in the DC regime ( $\tau \gg \max\{1, \gamma^2\}$ ),

$$g^{(2)}(r) = 1 + e^{-(r\sqrt{2\pi}/\Lambda_T)^2} - \sqrt{\frac{2\pi\gamma^2}{\tau}} \operatorname{erfc}\left(\frac{r\sqrt{2\pi}}{\Lambda_T}\right). \quad (39)$$

This is written in terms of the thermal de Broglie wavelength,

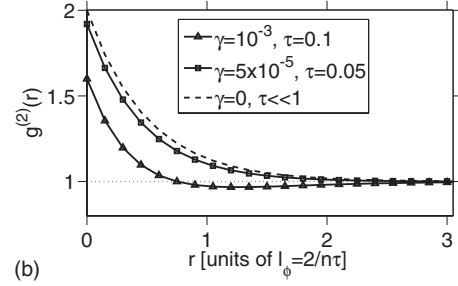
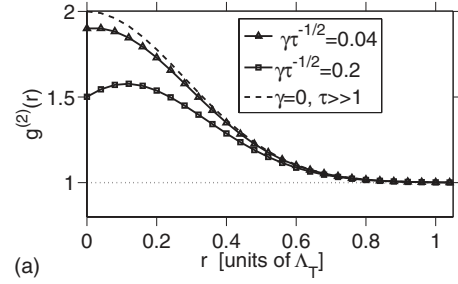


FIG. 1. Nonlocal pair correlation  $g^{(2)}(r)$  in the nearly ideal-gas regime: (a) decoherent classical regime,  $\tau \gg \max\{1, \gamma^2\}$  [Eq. (39)], with  $r$  in units of the thermal de Broglie wavelength  $\Lambda_T = \sqrt{4\pi/(\pi^2)}$  and (b) decoherent quantum regime,  $\sqrt{\gamma} \ll \tau \ll 1$  [Eq. (45)], with  $r$  in units of the phase coherence length  $l_\phi = 2/n\tau$ .

$$\Lambda_T = \sqrt{\frac{2\pi\hbar^2}{mT}} = \sqrt{\frac{4\pi}{\pi^2}}, \quad (40)$$

a quantity that will appear repeatedly in what follows. At  $r=0$  we have  $g^{(2)}(0) = 2 - \gamma\sqrt{2\pi}/\tau$  in agreement with Ref. [30]. In the noninteracting limit ( $\gamma=0$ ) we recover the well-known result for the classical ideal gas [59] characterized by Gaussian decay with a correlation length  $\Lambda_T$ . For  $\gamma > 0$  we observe [see Fig. 1(a)] the emergence of anomalous behavior, with a global maximum  $g^{(2)}(r_{\text{max}}) = g^{(2)}(0) + 2\gamma^2/\tau$  at nonzero interparticle separation  $nr_{\text{max}} = 2\gamma/\tau \ll 1$ . This corresponds to the emergence of antibunching,  $g^{(2)}(0) < g^{(2)}(r_{\text{max}})$ , due to repulsive interactions. As  $\gamma$  is increased further, there is a continuous transition from the DC regime to the regime of high-temperature “fermionization” (see Sec. VI B), with  $g^{(2)}(0)$  reducing further and the maximum moving to larger distances.

### C. Decoherent quantum regime

For temperatures below quantum degeneracy, with  $\sqrt{\gamma} \ll \tau \ll 1$ , only  $\omega_n=0$  contributes to the Green's function,

$$G_k(\sigma) = -T[\hbar^2 k^2/(2m) + |\mu|]^{-1}, \quad (41)$$

which gives the relation between the density and the chemical potential  $n = T\sqrt{m/(2\hbar^2|\mu|)}$ ,  $\mu = -|\mu|$ . Performing the Fourier transform of Eq. (41) one obtains the one-particle density matrix for the ideal gas,

$$g_{\text{ideal}}^{(1)}(r) = \langle \hat{\Psi}^\dagger(0) \hat{\Psi}(r) \rangle / n = \exp(-r/l_\phi), \quad (42)$$

which characterizes the decay of phase coherence over a length scale given by

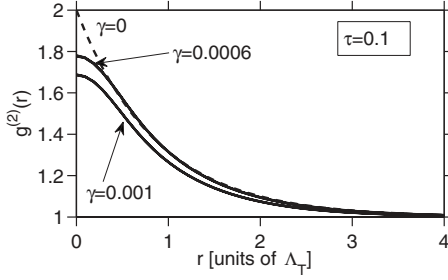


FIG. 2. Approach of the pair correlation function to the ideal-gas solution (shown dashed) in the decoherent quantum regime at  $\tau=0.1$ , with  $r$  in units of the thermal de Broglie wavelength,  $\Lambda_T = \sqrt{4\pi/m^2}$ . The thickness of the solid lines (numerical results) comes from the superimposed  $1\sigma$  error bars which are below resolution.

$$l_\phi = \frac{\hbar^2}{2m|\mu|} = \frac{2}{n\tau} \quad (43)$$

and also determines the second-order correlation function for the ideal gas

$$g_{\text{ideal}}^{(2)}(r) = 1 + |g_{\text{ideal}}^{(1)}(r)|^2 = 1 + e^{-2r/l_\phi}. \quad (44)$$

The one-particle Green's function [Eq. (41)] together with Eq. (33) leads to  $\Gamma(k, \sigma) = 4n^2 l_\phi / (k^2 l_\phi^2 + 4)$ . Inserting it into Eq. (32) we obtain (see Appendix B) corrections to  $g_{\text{ideal}}^{(2)}(r)$ , leading to the following result for the pair correlation function in the DQ regime:

$$g^{(2)}(r) = 1 + \left[ 1 - \frac{4\gamma}{\tau^2} \left( 1 + \frac{2r}{l_\phi} \right) \right] e^{-2r/l_\phi}. \quad (45)$$

This has the maximum value  $g^{(2)}(0) = 2 - 4\gamma/\tau^2$ , in agreement with the result in Ref. [30]. For  $\gamma=0$  the correlations decay exponentially with the characteristic correlation length of half a phase coherence length describing the long-wavelength phase fluctuations.

An interesting feature in this regime is the apparent prediction of weak antibunching at a distance as seen in Fig. 1(b), with  $g^{(2)}(r_{\min}) < 1$ . The strongest antibunching in expression (45) occurs at  $nr_{\min} = \tau/4\gamma \gg 1$  or  $r_{\min} = l_\phi \tau^2/4\gamma \gg l_\phi$  and dips below unity by an amount  $(4\gamma/\tau^2) \exp(-\tau^2/4\gamma) \ll 1$ . However, there is ambiguity regarding its existence: one should note that the dip below unity is very small in the region of uncontested validity of Eq. (45) where  $\tau/\sqrt{\gamma} \gg 1$  and only becomes appreciable around  $\tau \approx 2\sqrt{\gamma}$ , which is in the crossover region into the quasicondensate (see Sec. V). Whether such anomalous antibunching survives higher order corrections in the small parameter  $\sqrt{\gamma}/\tau$  remains to be seen. Our numerical calculations to date have not been able to access a regime of small enough  $\sqrt{\gamma}/\tau$  to confirm or deny its existence.

The numerical examples shown in Fig. 2 are for  $\sqrt{\gamma}/\tau \approx 0.24$  and  $\sqrt{\gamma}/\tau \approx 0.77$  and show a thermal bunching peak with a typical Gaussian shape at the shortest range of  $\Lambda_T$ , with  $\Lambda_T \ll l_\phi$ . At longer ranges, phase coherence dominates this and leads to exponential decay on the length scale  $l_\phi$ , in agreement with Eq. (45).

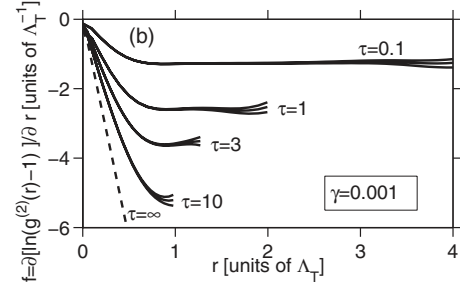
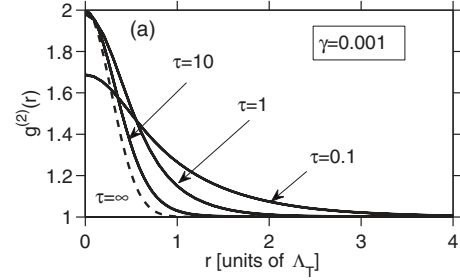


FIG. 3. Exact behavior of  $g^{(2)}(r)$ , with  $r$  in units of  $\Lambda_T$ , in the nearly ideal-gas regime with  $\gamma=0.001$  and varying  $\tau$  around the quantum/classical crossover. In panel (b), the derivative  $f = d[\ln(g^{(2)}(r)-1)]/dr$  shows a clear distinction between exponential decay (when  $f$  is constant) and Gaussian thermal-like behavior when  $f$  is linear. The triple lines indicate the numerical curves together with  $1\sigma$  error bars which are mostly below resolution.

#### D. Quantum/classical transition

The transition from the quantum to the classical decoherent gas was investigated using the gauge- $P$  numerical method. The behavior is shown in Figs. 2–5.

With rising temperature, still below degeneracy, one first finds a rounding off of the exponential behavior at short ranges of a fraction of  $\Lambda_T$ , as seen in Fig. 2. There is also a global lowering of  $g^{(2)}(r)$  with  $\gamma$ . It should be noted that the parameters for the numerical results shown in Fig. 2 are not deep in the regime where Eq. (45) applies accurately and the lowering of the tails with  $\gamma$  is weaker here than predicted by that limiting expression.

Considering variation with  $T$ , as temperature approaches and then exceeds  $T_d$ , Gaussian thermal-like behavior appears first at short ranges, progressively taking over an ever larger

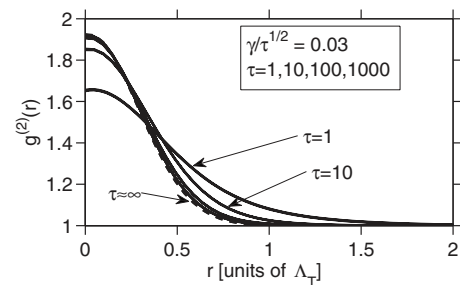


FIG. 4. Approach to the classical decoherent gas solution (shown dashed) [Eq. (39)] for finite but small interaction with  $\gamma/\sqrt{\tau}=0.03$ , which corresponds to a variation in density while keeping the coupling  $g$  and  $T$  constant. Here  $g^{(2)}(0) \rightarrow 1.925$  in the  $\tau \rightarrow \infty$  or equivalently  $n \rightarrow 0$  limit. Triple solid lines are the numerical results, with  $1\sigma$  error bars below resolution.



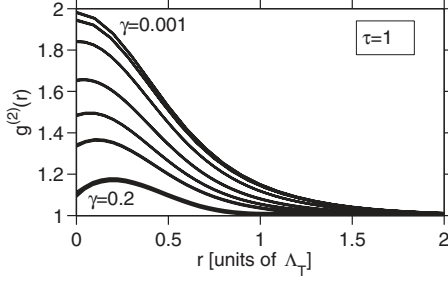


FIG. 5. Behavior of  $g^{(2)}(r)$  in the crossover region between decoherent classical and quantum gas at  $\tau=1$ . Values of  $\gamma$  shown are 0.001, 0.003, 0.01, 0.03, 0.06, 0.1, and 0.2 as the curves for  $g^{(2)}(r)$  descend.

part of  $g^{(2)}(r)$  as temperature is raised. This is seen in Fig. 3. The exponential tails can persist at ranges  $r \geq \Lambda_T / \sqrt{2\pi}$  well into the high-temperature regime when  $\gamma$  is small, as seen in Fig. 3(b) for  $\tau=3$  and even  $\tau=10$ .

There are three scenarios that can typically be controlled in ultracold gas experiments: (i) varying the absolute temperature changes  $\tau$  but not  $\gamma$ , as in Fig. 3; (ii) varying the coupling strength via a Feshbach resonance or varying the width of the trapping potential affects  $\gamma$  but not  $\tau$ , as considered in Sec. VII and Fig. 2; and (iii) varying the linear density gives changes in both  $\gamma$  and  $\tau$ , while keeping the quantity  $\gamma/\sqrt{\tau}$  constant. Notably, this is the parameter that appears in the analytic expressions for both decoherent regimes [Eqs. (39) and (45)].

Figure 4 shows the behavior under scenario (iii), where increasing  $\tau$  corresponds to decreasing density of the gas. As expected,  $g^{(2)}(0)$  tends to a constant value  $g^{(2)}(0)=2 - \gamma\sqrt{2\pi}/\tau \neq 2$  with  $\tau \rightarrow \infty$  predicted by Eq. (39). Interestingly, the crossover is quite broad under changing density, with departures from the decoherent classical result still visible at  $\tau \sim 100$ .

Finally, in the middle of the crossover region at  $\tau=1$ ,  $\gamma \ll 1$ , there is the smooth and quite broad transition from low values of  $\gamma$  to  $\gamma \sim \mathcal{O}(1)$  that is shown in Fig. 5. The situation of a short-range Gaussian with standard deviation  $\sim \Lambda_T/2\sqrt{\pi}$  and exponential tails with length scale  $l_\phi/2$  that was seen in Fig. 3 morphs into an anomalous form with a local maximum that is similar to the high-temperature fermionization behavior described below in Secs. VI and VII.

## V. WEAKLY INTERACTING QUASICONDENSATE REGIME [ $\tau^2 \ll \gamma \ll 1$ ]

In the regime of weak interactions and low temperature (or Gross-Pitaevskii regime) with  $\gamma \ll 1$  we rely on the fact that the equilibrium state of the gas is that of a quasicondensate [60,61]. In this regime the density fluctuations are suppressed while the phase still fluctuates. The pair correlation function is close to 1 and the deviations can be calculated using the Bogoliubov theory. In this approach, the field operator  $\hat{\Psi}$  is represented as a sum of the (*c*-number) macroscopic component  $\Psi_0$ , containing excitations with momenta  $k \leq k_0 \ll \xi^{-1}$  (where  $\xi = \hbar/\sqrt{mgn}$  is the healing length) and a

small operator component  $\delta\hat{\Psi}$  describing excitations with larger momenta,  $\hat{\Psi} = \Psi_0 + \delta\hat{\Psi}$ . The momentum  $k_0$  is chosen such that most of the particles are contained in  $\Psi_0$ ; however, its details do not enter into the lowest order corrections to  $g^{(2)}(r)$ , which are  $O(\delta\hat{\Psi})^2$ . Using Wick's theorem and the property of the thermal density matrix that  $\langle \delta\hat{\Psi} \rangle = 0$ , the pair correlation function is then reduced to

$$g^{(2)}(r) \simeq 1 + \frac{2}{n} [\text{Re} \langle \delta\hat{\Psi}^\dagger(r) \delta\hat{\Psi}(0) \rangle + \text{Re} \langle \delta\hat{\Psi}(r) \delta\hat{\Psi}(0) \rangle]. \quad (46)$$

The normal and anomalous averages  $\langle \delta\hat{\psi}^\dagger(r) \delta\hat{\psi}(0) \rangle$  and  $\langle \delta\hat{\psi}(r) \delta\hat{\psi}(0) \rangle$  are calculated using the Bogoliubov transformation,

$$\delta\hat{\psi}(r) = \frac{1}{L} \sum_k (u_k \hat{a}_k e^{ikx} - v_k \hat{a}_k^\dagger e^{-ikx}), \quad (47)$$

where  $L$  is the length of the quantization box,  $\hat{a}_k$  and  $\hat{a}_k^\dagger$  are the annihilation and creation operators of elementary excitations, and  $(u_k, v_k)$  are the expansion coefficients given by

$$u_k = \frac{\epsilon_k + E_k}{2\sqrt{\epsilon_k E_k}}, \quad v_k = \frac{\epsilon_k - E_k}{2\sqrt{\epsilon_k E_k}} \quad (48)$$

and satisfying  $u_k^2 - v_k^2 = 1$ . Here  $\epsilon_k = \sqrt{E_k(E_k + 2gn)}$  is the Bogoliubov excitation energy,  $E_k = \hbar^2 k^2 / (2m)$ , and we note that the following useful relationships between  $E_k$  and  $\epsilon_k$  hold:

$$E_k = \sqrt{\epsilon_k^2 + (gn)^2} - gn, \quad (49)$$

$$\frac{E_k}{\epsilon_k} = \left[ \frac{k^2}{k^2 + (2/\xi)^2} \right]^{1/2}, \quad (50)$$

where  $\xi = \hbar/\sqrt{mgn}$  is the healing length. The equilibrium occupation numbers of the Bogoliubov excitations are given by  $\bar{n}_k = \langle \hat{a}_k^\dagger \hat{a}_k \rangle = [e^{\epsilon_k/T} - 1]^{-1}$ .

Applying the Bogoliubov transformation to the normal and anomalous averages in Eq. (46) gives

$$g^{(2)}(r) = 1 + \frac{1}{\pi n} \int_{-\infty}^{+\infty} dk \cos(kr) [(u_k - v_k)^2 \bar{n}_k + v_k(v_k - u_k)]. \quad (51)$$

Using next Eq. (48) for the coefficients  $u_k$  and  $v_k$  we obtain the following result for the pair correlation function:

$$g^{(2)}(r) = 1 + \frac{1}{2\pi n} \int_{-\infty}^{+\infty} dk \left[ \frac{E_k}{\epsilon_k} (2\bar{n}_k + 1) - 1 \right] \cos(kr). \quad (52)$$

For convenience, we split the  $g^{(2)}(r)$  function into two parts corresponding to the contributions of thermal and vacuum fluctuations,

$$g^{(2)}(r) = 1 + G_0(r) + G_T(r), \quad (53)$$

with

$$G_0(r) = \frac{1}{2\pi n} \int_{-\infty}^{+\infty} dk \left[ \frac{E_k}{\epsilon_k} - 1 \right] \cos(kr) \quad (54)$$

and

$$G_T(r) = \frac{1}{\pi n} \int_{-\infty}^{+\infty} dk \frac{E_k}{\epsilon_k} \tilde{n}_k \cos(kr). \quad (55)$$

We first evaluate the vacuum contribution  $G_0(r)$  [Eq. (54)]. As shown in Appendix C, the integral in Eq. (54) can be obtained exactly in terms of special functions, giving

$$G_0(r) = -\sqrt{\gamma} [\mathbf{L}_{-1}(2\sqrt{\gamma}nr) - I_1(2\sqrt{\gamma}nr)], \quad (56)$$

where  $\mathbf{L}_{-1}(x)$  is the modified Struve function and  $I_1(x)$  is a Bessel function. The correlation length scale here is set by the healing length  $\xi = \hbar / \sqrt{mgn} = 1 / \sqrt{\gamma n}$ .

### A. Quasicondensate at low temperatures

At very low temperatures when the excitations are dominated by vacuum fluctuations, whereas the thermal fluctuations are a small correction, the  $G_T(r)$  term is calculated as follows. First, we substitute the explicit expression for  $\tilde{n}_k$  into Eq. (55), giving

$$G_T(r) = \frac{1}{\pi n} \int_{-\infty}^{+\infty} dk \frac{E_k}{\epsilon_k} \frac{1}{e^{\epsilon_k/T} - 1} \cos(kr). \quad (57)$$

As shown in Appendix C, for  $T \ll gn$  (or  $\tau \ll \gamma$ ), the integral can be simplified and gives

$$G_T(r) \approx \frac{\pi}{2\sqrt{\gamma}} \left[ \frac{1}{n^2 \pi^2 r^2} - \frac{\tau^2}{4\gamma} \operatorname{cosech}^2 \left( \frac{\pi \tau nr}{2\sqrt{\gamma}} \right) \right]. \quad (58)$$

Combining Eqs. (53), (56), and (58) we obtain the following final result for this regime ( $\tau \ll \gamma \ll 1$ ):

$$g^{(2)}(r) = 1 - \sqrt{\gamma} [\mathbf{L}_{-1}(2r/\xi) - I_1(2r/\xi)] + \frac{\sqrt{\gamma} \xi^2}{2\pi r^2} - \frac{\pi \tau^2}{8\gamma^{3/2}} \sinh^{-2} \left( \frac{\pi \tau r}{2\gamma \xi} \right). \quad (59)$$

In the limit of  $\tau \rightarrow 0$ , the terms in the second line of Eq. (59) cancel each other and the large-distance ( $r \gg \xi$ ) asymptotics of the difference of special functions  $\mathbf{L}_{-1}(x) - I_1(x) \sim 1/8\pi x^2$  ensure the expected inverse square decay of correlations [9]. At small but finite temperatures, the same large-distance asymptotics exactly cancel the inverse square behavior in the second line of Eq. (59) leaving only the exponential decay,

$$g^{(2)}(r) \xrightarrow{r \rightarrow \infty} 1 - \frac{\pi \tau^2}{8\gamma^{3/2}} e^{-\pi \tau r / \gamma \xi}, \quad (60)$$

to the uncorrelated value of  $g^{(2)}(r)=1$ . This is again in full agreement with the Luttinger liquid theory [9]. We note that even at  $T=0$ , oscillating terms are absent, in contrast to the strongly interacting regime of Sec. VI C [Eq. (71)]. The limit  $r \rightarrow 0$  in Eq. (59) reproduces the result of Eq. (9) in Ref. [30],  $g^{(2)}(0) = 1 - 2\sqrt{\gamma} / \pi + \pi \tau^2 / (24\gamma^{3/2})$ . In Fig. 6(a) we plot Eq.

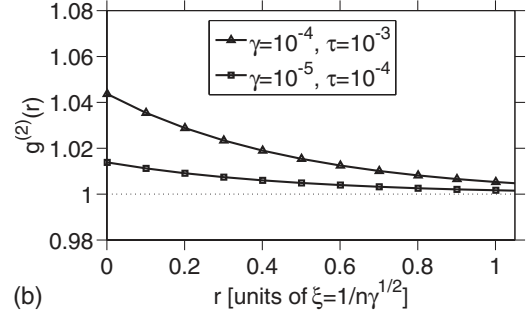
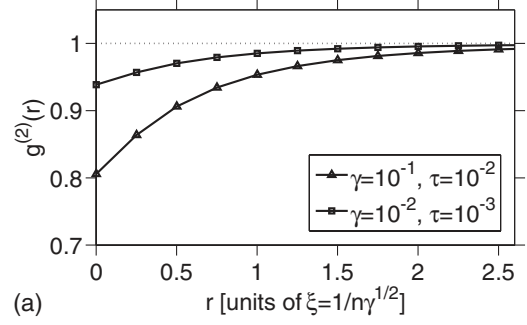


FIG. 6. Nonlocal pair correlation  $g^{(2)}(r)$  in the weakly interacting regime, with  $r$  in units of the healing length  $\xi = 1/\sqrt{\gamma n}$ : (a) low-temperature weakly interacting gas at  $\tau \ll \gamma \ll 1$  [Eq. (59)] and (b) weakly interacting gas at  $\gamma \ll \tau \ll \sqrt{\gamma}$  [Eq. (62)].

(59) for different values of the interaction parameter  $\gamma$ , and we note that the finite temperature correction term is negligible here.

### B. Thermally excited quasicondensate

In the opposite limit, dominated by thermal rather than vacuum fluctuations and corresponding to  $\gamma \ll \tau \ll \sqrt{\gamma}$ , the thermal part of the pair correlation function is calculated as follows. We first note that large thermal fluctuations correspond to  $\tilde{n}_k \gg 1$ , which in turn requires  $\epsilon_k/T \ll 1$ . Thus, we replace  $\tilde{n}_k$  in integral (55) by  $\tilde{n}_k = [\exp(\epsilon_k/T) - 1]^{-1} \approx T/\epsilon_k \gg 1$ . With this substitution, the integral for  $G_T(r)$  is dominated by the free-particle (quadratic in  $k$ ) part of the Bogoliubov spectrum and the calculations in Appendix C yield

$$G_T(r) = \frac{\tau}{2\sqrt{\gamma}} e^{-2\sqrt{\gamma}nr}. \quad (61)$$

This result is valid for  $r/\xi \lesssim 1$ . For  $r/\xi \gg 1$  the main contribution to the integral in Eq. (55) comes from the phonon (linear in  $k$ ) part of the Bogoliubov spectrum and one recovers the behavior given by Eq. (60).

Combining Eqs. (53), (56), and (61) we obtain the following final result for this regime ( $\gamma \ll \tau \ll \sqrt{\gamma}$  and  $r \lesssim \xi$ ):

$$g^{(2)}(r) = 1 + \frac{\tau}{2\sqrt{\gamma}} e^{-2r/\xi} - \sqrt{\gamma} [\mathbf{L}_{-1}(2r/\xi) - I_1(2r/\xi)]. \quad (62)$$

The last two terms are due to vacuum fluctuations and are a negligible correction here, so the leading term gives an exponential decay of correlations [see Fig. 6(b)] with a characteristic correlation length given by the healing length

$\xi = 1/\sqrt{\gamma n}$ . The peak value at  $r=0$  is  $g^{(2)}(0) = 1 + \tau/(2\sqrt{\gamma})$ , in agreement with Ref. [30].

## VI. STRONGLY INTERACTING REGIME [ $\gamma \gg \max\{1, \sqrt{\tau}\}$ ]

### A. Perturbation theory in $1/\gamma$

By mapping the system onto that of a weakly attractive 1D fermion gas [62] one can perform perturbation theory in  $1/\gamma \ll 1$ . The formalism is the same as in Sec. IV A except that  $\Psi$  is now a fermionic field and the interaction term in Hamiltonian (2) has to be modified to describe effective attractive interaction between fermions with matrix elements (in  $k$  space)  $V_k = -2\hbar^2 k^2 / (mn\gamma)$  [62]. Then

$$g^{(2)}(r) = g_{\gamma=\infty}^{(2)}(r) + \Delta g^{(2)}(r)$$

with  $g_{\gamma=\infty}^{(2)}(r) = 1 - e^{-n^2 \pi^2 r^2 / 2}$ . The first-order corrections to  $g^{(2)}(r)$  are given by the Hartree-Fock approximation as a sum of the direct and exchange contributions,

$$\Delta g_d^{(2)}(r) = \int_0^\beta d\sigma \int \frac{dk}{2\pi} V_k \Gamma(k, \sigma, r=0) \Gamma(-k, \sigma, r=0) e^{ikr}, \quad (63)$$

$$\Delta g_e^{(2)}(r) = - \int_0^\beta d\sigma \int \frac{dk}{2\pi} V_k \Gamma(k, \sigma, r) \Gamma(-k, \sigma, -r) e^{ikr}, \quad (64)$$

where

$$\Gamma(k, \sigma, r) = \int dp G_{p+k}(\sigma) G_p(-\sigma) e^{ipr} / 2\pi \quad (65)$$

in terms of the Green's function  $G_k(\sigma)$  for free fermions.

### B. Regime of high-temperature fermionization

We proceed with evaluation in the regime of high-temperature fermionization at temperatures well above quantum degeneracy,  $\tau \gg 1$ . In this regime, we use the Maxwell-Boltzmann distribution of quasimomenta as the unperturbed state. In the temperature interval  $1 \ll \tau \ll \gamma^2$ , the characteristic distance related to the interaction between the particles—the 1D scattering length  $a_{1D} = \hbar^2 / mg \approx l_\perp^2 / a \sim 1/\gamma n$ —is much smaller than the thermal de Broglie wavelength  $\Lambda_T$ , and the small perturbation parameter is  $a_{1D}/\Lambda_T \ll 1$  [30].

From the same formalism as in Sec. IV A, the free fermion Green's function is now given by

$$G_k(\sigma) = \begin{cases} \exp[(\beta + \sigma)(\mu - \hbar^2 k^2 / 2m)], & -\beta < \sigma < 0 \\ -\exp[\mu\sigma - \sigma \hbar^2 k^2 / 2m], & 0 < \sigma < \beta, \end{cases} \quad (66)$$

so the integral for  $\Gamma(k, \sigma, r)$  [Eq. (65)] gives

$$\Gamma(k, \sigma, r) = -n e^{-\sigma(\beta - \sigma)\hbar^2 k^2 / 2m} e^{-mr^2 / (2\hbar^2 \beta)} e^{-ikr\sigma / \beta}. \quad (67)$$

Substituting Eq. (67) into Eqs. (63) and (64) we obtain (see Appendix D)

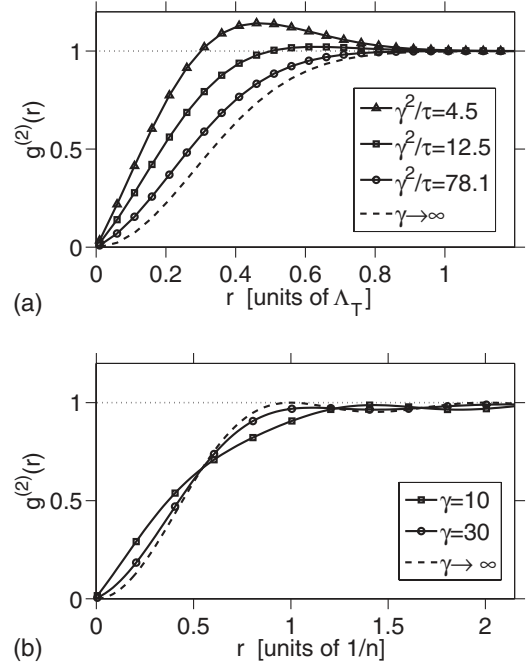


FIG. 7. Nonlocal pair correlation  $g^{(2)}(r)$  as a function of the relative distance  $r$  in the strongly interacting regime,  $\gamma \gg 1$ : (a) regime of high-temperature fermionization,  $1 \leq \tau \leq \gamma^2$  [Eq. (70)], with  $r$  in units of the thermal de Broglie wavelength  $\Lambda_T = \sqrt{4\pi}/(\pi^2)$  and (b) low-temperature Tonks-Girardeau regime [Eq. (71)] for  $\tau = 0.01$ , with  $r$  in units of mean interparticle separation  $1/n$ .

$$\Delta g_d^{(2)}(r) = \frac{2\pi|r|}{\gamma} e^{-n^2 \pi^2 r^2 / 2} - \frac{4}{n\gamma} \delta(r), \quad (68)$$

$$\Delta g_e^{(2)} = \frac{4}{n\gamma} \delta(r). \quad (69)$$

The only effect of the exchange contribution  $\Delta g_e^{(2)}$  is to cancel the delta function in the direct contribution. This leaves us with the following result for the pair correlation function in the regime of high-temperature fermionization ( $1 \leq \tau \leq \gamma^2$ ):

$$g^{(2)}(r) = 1 - \left[ 1 - 4 \sqrt{\frac{\pi\tau}{\gamma^2}} \left( \frac{r}{\Lambda_T} \right) \right] e^{-(r\sqrt{2\pi}/\Lambda_T)^2}. \quad (70)$$

In the limit  $r \rightarrow 0$  this leads to perfect antibunching,  $g^{(2)}(0) = 0$ , while the small finite corrections (as in Ref. [30],  $g^{(2)}(0) = 2\tau/\gamma^2$ ) are reproduced at order  $\gamma^{-2}$ . The correlation length associated with the Gaussian decay of correlations in Eq. (70) is given by thermal de Broglie wavelength  $\Lambda_T = \sqrt{4\pi}/(\pi^2)$ . For not very large  $\gamma$ , the correlations do not decay in a simple way but instead show an anomalous non-monotonic behavior with a global maximum at  $r_{\max} \approx \gamma/2\pi$ . This originates from the effective Pauli-type blocking at short range and thermal bunching [ $g^{(2)}(r) > 1$ ] at long range. As  $\gamma$  is increased the position of the maximum diverges and its value approaches 1 in a nonanalytical way  $g^{(2)}(r_{\max}) \approx 1 + (4\tau/\gamma^2) \exp(-\gamma^2/8\tau)$ .

Figure 7(a) shows a plot of Eq. (70) for various ratios of  $\gamma^2/\tau$ . For a well-pronounced global maximum, moderate val-

ues of  $\gamma^2/\tau$  are required (such as  $\gamma^2/\tau \approx 5$ , with  $\tau=8$ ,  $\gamma=6$ ), and these lie near the boundary of validity ( $\gamma^2/\tau \gg 1$ ) for our perturbative result in the high-temperature fermionization regime. Exact numerical calculations described in Ref. [34] and in more detail below in Sec. VII do, however, show qualitatively similar global maxima.

### C. Zero- and low-temperature (Tonks-Girardeau) regimes

At  $T=0$  the procedure is straightforward [42] and yields the known [8,42] result,

$$g_{T=0}^{(2)}(r) = 1 - \frac{\sin^2(\zeta)}{\zeta^2} - \frac{4 \sin^2(\zeta)}{\gamma \zeta^2} - \frac{2\pi}{\gamma} \frac{\partial}{\partial \zeta} \frac{\sin^2(\zeta)}{\zeta^2} + \frac{2}{\gamma} \frac{\partial}{\partial \zeta} \left[ \frac{\sin(\zeta)}{\zeta} \int_{-1}^1 dt \sin(\zeta t) \ln \frac{1+t}{1-t} \right], \quad (71)$$

where  $\zeta \equiv \pi nr$ . The last term here diverges logarithmically with  $\zeta$  and can be regarded as a first-order perturbation correction to the fermionic inverse square power law. Accordingly, Eq. (71) is valid for  $\zeta \ll \exp(\gamma)$ .

At temperatures well below quantum degeneracy,  $\tau \ll 1$ , finite temperature corrections to Eq. (71) are obtained using a Sommerfeld expansion around the zero temperature Fermi-Dirac distribution for the quasimomenta. For  $m \ll \tau^{-1}$  this gives an additional contribution of  $\tau^2 \sin^2(\pi nr)/12\pi^2$  to the right-hand side of Eq. (71), which is negligible compared to the  $T=0$  result as  $\tau \ll 1$ . At  $r=0$ , Eq. (71) gives perfect antibunching  $g^{(2)}(0)=0$ , which corresponds to a fully “fermionized” 1D Bose gas, where the strong interatomic repulsion mimics the Pauli exclusion principle for intrinsic fermions. By extending the perturbation theory to include terms of order  $\gamma^{-2}$  we can reproduce the known result for the local pair correlation at zero temperature  $g^{(2)}(0)=4\pi^2/3\gamma^2$  [29,30].

In Fig. 7(b) we plot the function  $g^{(2)}(r)$  [Eq. (71)] for various  $\gamma$ . According to the physical interpretation of the pair correlation function  $g^{(2)}(r)$ , its oscillatory structure, and hence the existence of local maxima and minima at certain finite values of  $r$ , implies that there exist more and less likely separations between the pairs of particles in the gas. This can be interpreted as a quasicrystalline order (with a period of  $\sim 1/n$ ) in the two-particle sector of the many-body wave function even though the density of the gas is uniform.

The oscillatory behavior of the pair correlation in this strongly interacting regime is similar to Friedel oscillations in the density profile of a 1D interacting electron gas with an impurity [63]. We also mention that our derivation of Eq. (71) is equally valid for strong attractive interactions, i.e., when  $\gamma < 0$  and  $|\gamma| \gg 1$ , and therefore it describes the pair correlations in a metastable state known as super-Tonks gas [64].

### D. Numerical results

Numerical calculations with the gauge- $P$  method are able to reach only the low- $\gamma$  (or, equivalently, high- $\tau$ ) edge of the high-temperature fermionization regime, however a comparison with Eq. (70) is instructive. In Fig. 8 we see that the length scale on which antibunching occurs is still qualita-

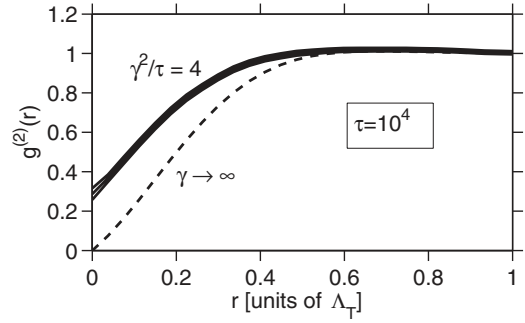


FIG. 8. Behavior on the verge of the high- $T$  fermionization regime for  $\gamma^2/\tau=4$ . The dashed line is Eq. (70).

tively given by Eq. (70) while any discrepancies are of the same size as at  $r=0$ . This is actually a general feature in all the parameter regimes explored by the numerics. Overall, the discrepancy between the  $1/\gamma$  perturbation expansions (39), (45), and (70) and the exact behavior of  $g^{(2)}(r)$  at nonzero  $r$  is roughly the same as at  $r=0$ . Since a calculation of  $g^{(2)}(0)$  [30] from the exact solution of the Yang-Yang integral equations [7] is usually more straightforward to evaluate than the full stochastic calculation of  $g^{(2)}(r)$ , it can serve as a useful guide to whether a numerical calculation is warranted or not.

## VII. CLASSICAL TO FERMIONIZATION TRANSITION AND CORRELATION MAXIMA

Figure 9 shows the behavior in the transition region between the decoherent classical and high-temperature fermionization regimes (found with the gauge- $P$  numerical method) when one is far above the degeneracy temperature  $T_d$ . One sees the appearance of a maximum in the correlations at finite range as the transition is approached. As pointed out in Sec. VI B, this arises from an interplay of thermal bunching and repulsive antibunching on comparable scales. A comparison of relevant length scales indicates that the  $\tau \approx \gamma^2$  here corresponds to  $\Lambda_T \sim a_{1D}$ , where  $a_{1D}$  is the “1D scattering length” that describes the asymptotic behavior of the wave function in two-body scattering.

An interesting behavior occurs in the crossover regime when  $\gamma^2/\tau \approx 0.1-0.4$ . Here we can have  $g^{(2)}(0)=1$  just like in the quasicondensate or “Gross-Pitaevskii” regime, indicating local second-order coherence. However, unlike the qua-

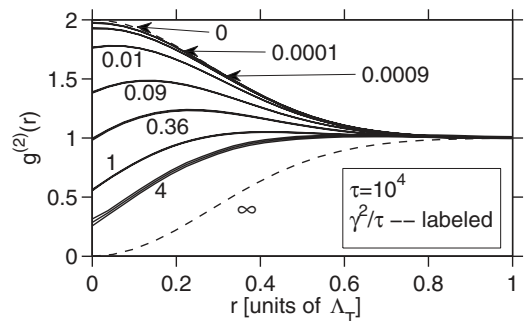


FIG. 9. Crossover from decoherent classical to high-temperature fermionization regimes at high temperature.



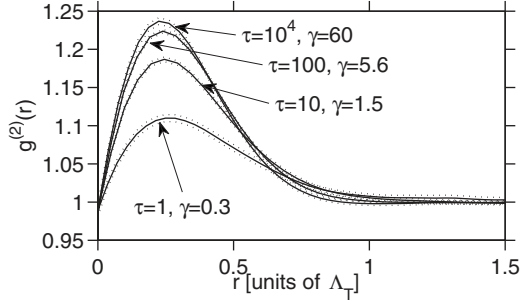


FIG. 10. Situation when  $T > T_d$  and the local second-order coherence is apparently unity. All curves plotted correspond to parameter values for which  $g^{(2)}(0) = 1$  in the crossover region between the classical decoherent and high-temperature fermionized gas. The dots (rather than triple lines here, for clarity) indicate  $1\sigma$  error bars.

scondensate regime, the nonlocal correlations on length scales of  $\sim \Lambda_T$  are *not* coherent and, in fact, appreciably bunched. This is shown in Fig. 10. It is a symptom of the broader correlation maximum phenomenon.

The height of this maximum for more general parameters is shown in Fig. 11 as a function of both  $g^{(2)}(0)$  and  $\gamma^2/\tau$ . One sees that this behavior is well pronounced in the crossover between high-temperature fermionization and decoherent classical regimes, peaking when  $g^{(2)}(0) \approx 1$  (a situation shown also in Fig. 10) or, equivalently,  $\gamma^2 \sim 0.3\tau$ . As one

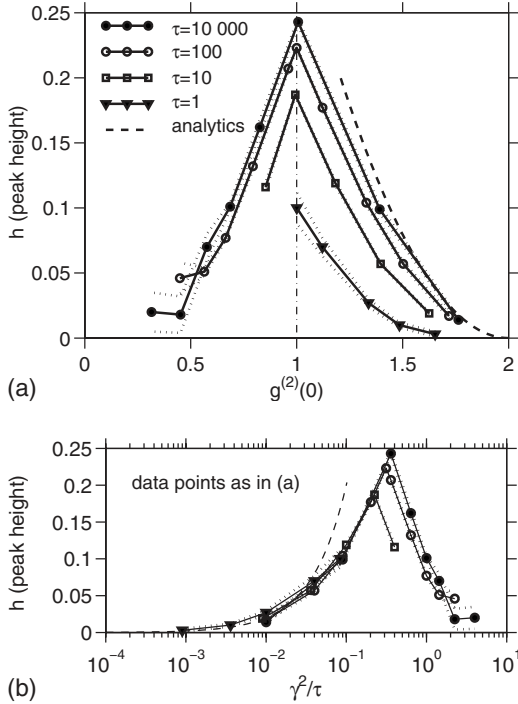


FIG. 11. Heights of the anomalous peak of  $g^{(2)}(r)$  that occurs at nonzero  $r_{\max}$ , for different values of  $\tau$ , as functions of (a)  $g^{(2)}(0)$  and (b)  $\gamma^2/\tau$ . The height is taken to be  $h \equiv g^{(2)}(r_{\max}) - g^{(2)}(0)$  at high temperatures when  $g^{(2)}(0) > 1$  and  $h \equiv g^{(2)}(r_{\max}) - 1$  when  $g^{(2)}(0) < 1$ . The two regimes are separated by the dotted-dashed vertical line in (a). Analytic results from Eq. (39) in the decoherent quantum regime are shown as a dashed line. Dots (rather than triple lines here, for clarity) indicate  $1\sigma$  error bars on the numerical results.

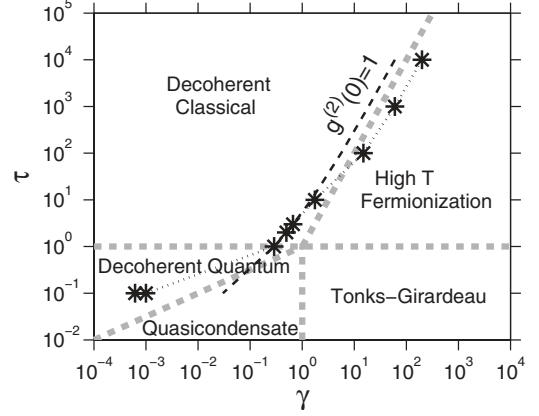


FIG. 12. Regimes and their numerical accessibility: the asterisks indicate the lowest  $\tau$  and highest  $\gamma$  reachable using the gauge- $P$  method as described in Appendix A. The dark dashed line indicates the point at which  $g^{(2)}(0) = 1$ .

reaches degenerate temperatures, the maximum peak height is reduced and presumably disappears completely by the time the quasicondensate regime is reached by going to smaller values of  $\gamma$ . Although we were unable to numerically reach the relevant quasicondensate region for  $\tau < 1$ , a more refined numerical setup that improves the importance sampling or the  $\mu(T)$  trajectory described in Appendix A may allow this.

## VIII. NUMERICAL LIMITATIONS

Figure 12 shows the regime that was accessible using the relatively straightforward numerical scheme that was employed here and detailed in Appendix A. (It is the region above and to the left of the asterisks.) In particular, one sees that of the physical regimes described in Secs. IV–VII, the decoherent classical, as well as parts of the decoherent quantum and high-temperature fermionization regimes were accessible, while the quasicondensate and Tonks-Girardeau regimes were not.

The principal difficulty that is encountered, generally speaking, is the growth of statistical noise with increasing  $\beta$ , i.e., decreasing  $\tau$ , which eventually prevents one from obtaining values of  $g^{(2)}(r)$  with a useful resolution. This arises in two different ways depending on the region of interest.

First, in the strongly interacting (fermionized) region, one needs a correspondingly large coupling constant  $g \propto \gamma$  which leads to a relative increase in the importance of the noise terms of the  $d\alpha_j^{(p)}/d\beta$  equations in Eq. (21). This leads to large statistical uncertainty in the  $\alpha_j^{(p)}$  themselves or to the weight  $\Omega$  whose evolution depends on them. The upshot is that the inverse temperature  $\beta$  at which the noise becomes unmanageable becomes smaller and smaller as  $\gamma$  grows. Technical improvements are unlikely to make a large dent in the problem in the fermionized regime because it ultimately stems from the fact that coherent states are no longer a good basis over which to expand the density matrix. They are not close to the preferred eigenstates of the system. Instead, one can think of constructing a phase-space distribution that uses



a noncoherent-state basis, for example, a Gaussian basis [65]. This general approach—together with symmetry projections—has been utilized in successfully calculating ground state properties of the strongly correlated fermionic Hubbard model [66].

Second, in the low  $\gamma$  and  $\tau$  region, one has a different underlying source of statistical uncertainty. The longest relevant length here is either the coherence length  $l_\phi$  or the healing length  $\xi$ , and for correct calculations in the large uniform gas one must simulate a system of a total size appreciably greater than these lengths. This in turn imposes a minimal total particle number,

$$N \geq \max[\mathcal{O}(4/\tau), \mathcal{O}(2/\sqrt{\gamma})]. \quad (72)$$

The thermal initial conditions of Eq. (12) lead to variation of  $N$  among trajectories, and since the Gibbs factor  $K$  [see Eq. (16)] grows linearly or faster with  $N$ , one also obtains a growing variation of  $K(\vec{v})$ . This enters the  $d\Omega$  of Eq. (21) and leads to a spread of the weights  $\Omega(t)$  that grows rapidly (note the exponential growth of  $\Omega$ ) with increasing  $N$ . However because of the long length scales, via Eq. (72), large  $N$  is needed to make accurate calculations when  $\tau$  or  $\gamma$  are much smaller than 1. The end result is domination of the whole calculation by one or a few trajectories with the highest weight for all realistic ensemble sizes  $\mathcal{S}$ .

As a corollary, significantly lower temperatures, even down to the quasicondensate regime, are *accessible* at small  $\gamma$  if one is prepared to sacrifice the assumption of an infinite-sized gas and consider periodic boundary conditions on some length  $L$  that is smaller than or comparable to the coherence/healing lengths. This approach was taken, e.g., in [67]. This stops the rise of overall particle number; hence one has a much smaller spread of Gibbs factors  $\Omega$  among the trajectories and in the final analysis—reduced statistical uncertainty. Such calculations are no longer as general, though, and are not considered in this paper.

We would like to point out that the limitation in this regime may be overcome or alleviated if the rather simplistic importance sampling used in the numerical method was to be improved. The leading candidate is an improved importance sampling algorithm, possibly using a Metropolis sampling procedure, as outlined at the end of Appendix A 3.

Finally, it is also possible that a more refined choice of  $\mu(\beta)$  (considered in Appendix A 5) may lead to somewhat improved coverage of the parameter space in general.

## IX. OVERVIEW AND CONCLUSION

In conclusion, we have surveyed the behavior of the spatial two-particle correlation function in a repulsive uniform 1D Bose gas. We have analyzed numerically the pair correlation functions for all relevant length scales, with the exception of several low-temperature transition regions (see Fig. 12 below the asterisks) which were not accessible by the numerical scheme we employed. Approximate analytic results and methods have been presented for parameters deep within all the major physical regimes. The key features of this behavior include:

(i) thermal bunching with  $g^{(2)}(0) \approx 2$  and Gaussian drop off at ranges  $\Lambda_T$  in the classical decoherent regime,

(ii) exponential drop off of correlations from  $g^{(2)}(0) \approx 2$  at ranges  $l_\phi$  in the decoherent quantum regime along with Gaussian-type rounding at shorter ranges  $\sim \Lambda_T$ ,

(iii) suppressed density fluctuations with  $g^{(2)}(0) \approx 1$  and exponential decay at ranges of the healing length  $\xi$  in the quasicondensate regime,

(iv) antibunching with  $g^{(2)}(0) < 1$  and Gaussian decay at ranges  $\Lambda_T$  in the high-temperature fermionization regime,

(v) antibunching with  $g^{(2)}(0) < 1$  and oscillatory decay on ranges of the mean interparticle separation  $1/n$  in the Tonks-Girardeau regime, and

(vi) bunching at a range of  $\sim 0.3\Lambda_T$  in the crossover between classical and fermionized regimes around  $\gamma^2 \sim 0.3\tau$ .

Let us consider the regimes in turn, starting from the classical decoherent gas, then going anticlockwise in Fig. 12. The classical decoherent gas is well approximated by Boltzmann statistics and is dominated by thermal fluctuations. The pair correlation function shows typical thermal bunching and a Gaussian decay, with the correlation length given by the thermal de Broglie wavelength  $\Lambda_T$ .

As one reduces the temperature, the gas becomes degenerate and the thermal de Broglie wavelength becomes larger than the mean interparticle separation and loses its relevance. The correlation length increases and one enters into the decoherent quantum regime. Here, the dominant behavior of the gas is the ideal Bose gas bunching,  $g^{(2)}(0) \approx 2$ , with large density fluctuations that decay exponentially on the length scale given by the phase coherence length  $l_\phi$ . Notably, the exponential behavior starts to appear well above degeneracy first in the long-distance tails, being visible even around  $\tau \sim 10$  as in Fig. 3.

Reducing the temperature even further, while still at  $\gamma \ll 1$ , one enters into the quasicondensate regime, in which the density fluctuations become suppressed and  $g^{(2)}(0) \approx 1$ . In the hotter subregime dominated by thermal fluctuations, the pair correlation shows weak bunching,  $g^{(2)}(0) > 1$ , while in the colder subregime dominated by quantum fluctuations one has weak antibunching,  $g^{(2)}(0) < 1$ . In both cases the pair correlation decays on the length scale of the healing length  $\xi$ .

We now move to the right on Fig. 12, into the regime of strong interactions, while staying at temperatures well below quantum degeneracy,  $\tau \ll 1$ . This is the Tonks-Girardeau regime, in which the density fluctuations get further suppressed due to strong interparticle repulsion. Antibunching increases and one approaches  $g^{(2)}(0) = 0$  due to fermionization. The only relevant length scale here is the mean interparticle separation,  $1/n$ , and the pair correlation function decays on this length scale with some oscillations.

We next move up on Fig. 12, to higher temperatures, and enter the regime of high-temperature fermionization. At short range, the pair correlation here is still antibunched due to strong interparticle repulsion, however, thermal effects start to show up on the length scale of  $\Lambda_T$ . As a result of these competing effects, the nonlocal pair correlation develops an anomalous peak, corresponding to bunching at a distance, with  $g^{(2)}(r_{\max}) > 1$ , beginning around  $\tau \sim \gamma^2/2$ .

As we increase the temperature even further, the thermal effects start to dominate over interactions and the antibunching dip gradually disappears. At temperatures  $\tau \sim \gamma^2$  we observe a crossover back to the classical decoherent regime.

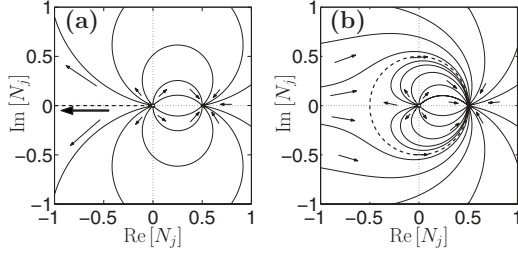


FIG. 13. Deterministic phase space for Stratonovich for the  $dN_j$  equation when  $\mu_e=0$ : (a) ungauged and (b) using gauge (A6). The moving singularity in (a) is shown with a large arrow and the attractor in (b) at  $|N_j|=N_a$  with a thick dashed line.

Our results provide insights into the fundamental understanding of the 1D Bose gas model through many-body correlations. Calculation of these nonlocal correlations is not accessible yet through the exact Bethe ansatz solutions. We expect that our theoretical predictions will serve as guidelines for future experiments aimed at the measurement of nonlocal pair correlations in quasi-1D Bose gases.

#### ACKNOWLEDGMENTS

A.G.S., M.J.D., P.D.D., and K.V.K. acknowledge fruitful discussions with A. Yu. Cherny and J. Brand and the support of this work by the Australian Research Council. D.M.G. acknowledges support by EPSRC. P.D. was supported by the European Community under Contract No. MEIF-CT-2006-041390. K.V.K., P.D., and D.M.G. thank IFRAF and the Institut Henri Poincaré–Centre Emile Borel for support during the 2007 Quantum Gases Workshop in Paris where part of this work was completed. LPTMS is a mixed research unit No. 8626 of CNRS and Université Paris-Sud.

#### APPENDIX A: TECHNICAL APPENDIX FOR THE GAUGE- $P$ CALCULATIONS

##### 1. Instability of the stochastic equations and its removal with a stochastic gauge

A straightforward application of the ungauged diffusion equations [Eq. (19)] is foiled by the presence of an instability in the  $d\alpha_j^{(v)}/d\beta$  equations. We can see this if we first consider the evolution of  $N_j$  and discard the noise and kinetic-energy parts of the equation. Taking the deterministic part from the Stratonovich calculus which is used for our numerics (this introduces the  $1/2$  term below), one has

$$\frac{\partial N_j}{\partial \beta} \sim N_j \left[ \mu_e - \frac{g}{\Delta x} \left( N_j - \frac{1}{2} \right) \right]. \quad (\text{A1})$$

There are stationary points at the vacuum  $N_j=0$  and at  $N_j=N_a=1/2+\mu_e\Delta x/g$ , with the more positive stationary point (usually  $N_a$ ) being an attractor and the more negative being a repeller [see Fig. 13(a)]. The deterministic evolution is easily solved, and starting from a time  $\beta_0$  gives later evolution as

$$N_j(\beta) = \frac{N_a N_j(\beta_0)}{N_j(\beta_0) + [N_a - N_j(\beta_0)] e^{-\mu_e(\beta-\beta_0)}}. \quad (\text{A2})$$

If it has a negative  $N_j(\beta_0)$ , which is possible due to the action of the noises  $\zeta$ , then at a later time

$$\beta_{\text{sing}} = \beta_0 + \frac{1}{\mu_e} \ln \left( 1 - \frac{N_a}{N_j(\beta_0)} \right), \quad (\text{A3})$$

the solution has diverged to negative infinity. This behavior of the deterministic part of the equations is known as a “moving singularity” and is a well-known indicator of non-vanishing boundary terms when an integration by parts is performed on the operator [Eq. (14)] [50,57]. It implies that FPE (18) is not fully equivalent to quantum mechanics.

The use of a stochastic gauge to remove this kind of instability has been described in [49] and in more detail in [50]. The gauge identity [Eq. (17)] can be used on Eq. (14) to introduce an arbitrary modification to the deterministic evolution (arising from first-order derivative terms) for the price of additional diffusion in the weight  $\Omega$ . Since the gauge identity is zero, we can add an arbitrary multiple of it to Eq. (14). In particular, if we add

$$0 = \int G(\vec{v}) \sum_j \left\{ \frac{\mathcal{G}_j^2 \Omega^2}{2} \frac{\partial^2}{\partial \Omega^2} + i \mathcal{G}_j \sqrt{\frac{g}{2\Delta x}} \sum_\nu \alpha_j^{(\nu)} \frac{\partial}{\partial \alpha_j^{(\nu)}} \right. \\ \left. \times \left( \Omega \frac{\partial}{\partial \Omega} - 1 \right) \right\} \hat{\Lambda} d^{4M+2} \quad (\text{A4})$$

with arbitrary functions  $\mathcal{G}_j(\vec{v}, \beta)$  and perform the subsequent steps as before, then the diffusion matrix in the resulting FPE remains positive semidefinite (no negative eigenvalues), and the resulting Ito diffusion equations of the samples become

$$\frac{d\alpha_j^{(\nu)}}{d\beta} = \frac{1}{2} \left( \mu_e + \frac{\hbar^2 \nabla^2}{2m} - \frac{g N_j}{\Delta x} \right) \alpha_j^{(\nu)} \\ + i \alpha_j^{(\nu)} [\zeta_j^{(\nu)}(\beta) - \mathcal{G}_j] \sqrt{\frac{g}{2\Delta x}},$$

$$\frac{d\Omega}{d\beta} = \Omega \left[ -K(\vec{v}) + \sum_j \mathcal{G}_j \sum_\nu \zeta_j^{(\nu)}(\beta) \right] \quad (\text{A5})$$

instead of Eq. (19). The  $\alpha_j$  equations are modified and compensating correlated noises have been added to the  $\Omega$  equation.

We now wish to choose the functions  $\mathcal{G}_j$ , called stochastic gauges, so that the instability is removed, keeping also in mind the goal of keeping the (now unbiased) statistical uncertainty manageable. Heuristic guidelines for choosing gauges have been investigated in detail in [50]. Several choices for a single-mode system were also investigated there in Sec. 9.2 of [50] in terms of resulting statistical uncertainties. The aim is to remove the real part of  $N_j$  from the  $\alpha_j$  equation when it is negative, so as to neutralize the moving singularity. While for a single mode the “radial” gauge was found to give the best performance, later tests that we have performed on the full multimode ( $M \gg 1$ ) 1D gas show that the “minimal” drift gauge

$$\mathcal{G}_j = i(\text{Re } N_j - |N_j|) \sqrt{\frac{g}{2\Delta x}} \quad (\text{A6})$$

gives better performance for this system. This is because it introduces the smallest modifications needed to remove the moving singularity and hence the smallest noise contributions to the weight  $\Omega$ . The weight becomes much more important for multimode systems because each of the  $M$  modes adds its own contribution to it, the total of which can become large. The phase-space modification for a single mode for the ungauged [Eq. (A1)] and gauged equations is shown in Fig. 13. One sees that in the “classical”  $\text{Re}[N_j] \gg \text{Im}[N_j]$  region the trajectories are practically unchanged. The final Ito equations to be integrated are Eq. (21). Comparisons to known exact results such as energy and density [7] and  $g^{(2)}(0)$  [30] indicate no deviations beyond what is predicted by the unbiased statistical uncertainties [Eq. (26)], using the gauged equations. Such a comparison can be seen in Fig. 2 of Ref. [34].

## 2. Integration procedure

The actual integration is performed using a split-step semi-implicit method described in [68], which requires the use of the Stratonovich stochastic calculus. There, it was shown to be highly superior to other low-order methods in terms of stability. Although a low-order Newton-type method, with the right choice of variables its performance is remarkably good. High-order methods such as Runge-Kutta or others suffer from serious complications when noise is present. In particular, one has to be very meticulous in tracking down and compensating for all the nonzero correlations within a single time step—these are much more complicated than the simplest correction terms appearing in the Stratonovich semi-implicit method used here.

Due to the multiplicative form of Eq. (21), it is highly advantageous to use logarithmic variables, which is made possible if one uses a split-step method. Here, a  $\Delta\beta$  time step consists of the following four stages: First the interaction part (containing  $g$ ) is integrated in real space over a time step  $\Delta\beta$ . Second, the fields are Fourier transformed to  $k$  space, giving  $\tilde{\alpha}^{(\nu)}(k)$ . Third the kinetic-energy contributions are integrated over  $\Delta\beta$ , and finally one Fourier transforms back into real space, ready to start the next time step. The Stratonovich gauged evolution equations for the real space stage are

$$\frac{d \ln \alpha_j^{(\nu)}}{d\beta} = -\frac{g}{2\Delta x} \left( |N_j| + i \text{Im } N_j - \frac{1}{2} \right) + i \zeta_j^{(\nu)}(\beta) \sqrt{\frac{g}{2\Delta x}}, \quad (\text{A7a})$$

$$\begin{aligned} \frac{d \ln \Omega}{d\beta} = & i \sqrt{\frac{g}{2\Delta x}} \sum_{j,\nu} (\text{Re } N_j - |N_j|) \zeta_j^{(\nu)}(\beta) \\ & + \frac{g}{2\Delta x} \sum_j \{ (\text{Re } N_j - |N_j|)^2 - N_j^2 + i \text{Im } N_j \}, \end{aligned} \quad (\text{A7b})$$

while for the  $k$ -space stage they are

$$\frac{d \ln \tilde{\alpha}^{(\nu)}(k)}{d\beta} = \frac{1}{2} \left[ \mu_e - \frac{\hbar^2 k^2}{2m} \right], \quad (\text{A7c})$$

$$\frac{d \ln \Omega}{d\beta} = \sum_k \left( \mu_e - \frac{\hbar^2 k^2}{2m} \right) \tilde{\alpha}^+(k) \tilde{\alpha}(k). \quad (\text{A7d})$$

## 3. Importance sampling

The simulated equations [Eq. (21)] include evolution of both the amplitudes  $\alpha_j^{(\nu)}$  and weight  $\Omega$ . This combination can cause sampling problems for observable estimations [Eq. (22)] when maximum weights occur for very rare trajectories. As it turns out, this was a serious issue for the majority of calculations reported here because while the initial distribution (12) samples the  $\beta=0$  system well, this is not necessarily the case during the later evolution into  $\beta \gg 0$  that is of most interest. Fortunately, fairly rudimentary importance sampling was able to deal with this for a wide range of parameters.

The essence of this approach is to preweight trajectories in such a way that the part of the distribution with maximum weight  $\Omega$  coincides with the majority of samples at the target time of interest  $\beta_t$  rather than at  $\beta=0$ . The price paid is that the  $\beta=0$  distribution is then poorly sampled, but this is not important to us as we are interested rather in the target  $\beta_t$ .

Prewighting is made possible because in all observable calculations [Eq. (22)], the combination  $[G(\vec{v})\Omega]$  occurs as a universal common factor in the  $\int d\vec{v}$  integral. Hence, if we manually scale the weight  $\Omega$  by some factor  $F(\vec{v})$  of our choice,  $\Omega \rightarrow \Omega' F(\vec{v})$ , and simultaneously rescale the distribution according to  $G(\vec{v}) \rightarrow G'(\vec{v})/F(\vec{v})$ , then with  $\Omega'$  and  $G'$  one obtains exactly the same results in the infinite-number-of-samples limit as with  $G\Omega$ . However, the actual samples are differently distributed, which is advantageous for finite sample numbers. To reduce the weight sampling problem, one wants to make such a modification  $F(\vec{v})$  that both  $G'(\vec{v})$  and  $\Omega' G'(\vec{v})$  peak in the same region of the phase space of  $\vec{v}$ .

To proceed, it is convenient to consider Fourier-transformed variables in  $k$  space, where the noninteracting evolution can be easily exactly solved. Define then

$$\tilde{\alpha}_k^{(\nu)} = \frac{1}{\sqrt{M}} \sum_j e^{-ikx_j} \alpha_j^{(\nu)} = \begin{cases} \tilde{\alpha}_k & \text{if } \nu = 1 \\ \tilde{\alpha}_k^+ & \text{if } \nu = 2, \end{cases} \quad (\text{A8})$$

where  $k$  takes on discrete values from  $-\pi/\Delta x$  to  $\pi/\Delta x$ . The “naive” initial distribution (12) then becomes

$$G_0(\vec{v}) = \delta^2(\ln \Omega) \prod_k \delta^2[\tilde{\alpha}_k - (\tilde{\alpha}_k^+)^*] \frac{e^{-|\tilde{\alpha}_k|^2/\bar{n}_x}}{\pi \bar{n}_x}. \quad (\text{A9})$$

This is a thermal distribution which is uniform over all  $k$ . The ideal gas (i.e.,  $g=0$ ) evolution of Eq. (21) then leads to

$$\tilde{\alpha}_k^{(\nu)}(\beta) = \tilde{\alpha}_k(0) \exp \left[ \left( \mu(\beta) - \frac{\hbar^2 k^2}{2m} \right) \frac{\beta}{2} \right],$$

$$\ln \Omega(\beta) = \sum_k (|\tilde{\alpha}_k(\beta)|^2 - |\tilde{\alpha}_k(0)|^2), \quad (\text{A10})$$

where

$$\tilde{\alpha}_k(0) = \sqrt{\bar{n}_x} \eta_k, \quad (\text{A11})$$

with  $\eta_k$  being independent complex Gaussian noises with variance unity,  $\langle \eta_k^* \eta_{k'} \rangle_S = \delta_{kk'}$ . One can see that Eq. (A10) is not necessarily anywhere near a well-sampled ideal-gas Bose-Einstein distribution at temperature  $\beta$ , which would have

$$\begin{aligned} \tilde{\alpha}_k^{(v)}(\beta) &= \sqrt{n_k^{\text{id}}(\beta)} \eta_k, \\ \ln \Omega(\beta) &= 0, \end{aligned} \quad (\text{A12})$$

with

$$n_k^{\text{id}}(\beta) = \{\exp[-\mu(\beta)\beta + \hbar^2 k^2 \beta / 2m] - 1\}^{-1}$$

being the usual Bose-Einstein distribution.

For the purpose of the simulations presented here, a fairly crude yet effective importance sampling was applied as follows. For relatively weak coupling  $g$ , a very rough but useful estimate of the thermal state at coarse resolution is that the Fourier modes are decoupled and thermally distributed with some mean occupations  $n_k(\beta_t)$  at the target time  $\beta_t$  that we are interested in. In practice we will choose some estimate of the guiding density  $n_k(\beta_t)$ . The desired equal weight sampling at time  $\beta_t$  would then correspond to the distribution

$$G^{\text{est}}(\vec{v}, \beta_t) = \delta^2(\ln \Omega) \prod_k \delta^2(\tilde{\alpha}_k - (\tilde{\alpha}_k^+)^*) \frac{\exp[-|\tilde{\alpha}_k|^2/n_k(\beta_t)]}{\pi n_k(\beta_t)}, \quad (\text{A13})$$

which leads to samples given by  $\tilde{\alpha}_k^{(v)} = \sqrt{n_k(\beta)} \eta_k$  and  $\Omega = 1$ . What we are interested in is the corresponding distribution of samples at  $\beta=0$ . An estimate of the initial distribution that leads to  $G^{\text{est}}(\vec{v}, \beta_t)$  can be obtained by evolving Eq. (A13) back in imaginary time using only kinetic interactions. This is again rather rough since deterministic interaction terms  $\propto g$  are omitted, not to mention noise, but it is simple to carry out and proved sufficient for our purposes here. One obtains then an estimated sampling distribution for samples at  $\beta=0$ ,

$$\begin{aligned} G^{\text{samp}}(\vec{v}, 0) &= \delta^2(\ln \Omega - \ln \Omega_0) \prod_k \delta^2[\tilde{\alpha}_k - (\tilde{\alpha}_k^+)^*] \\ &\times \frac{\exp(-|\tilde{\alpha}_k|^2/n_k^{\text{samp}})}{\pi n_k^{\text{samp}}}, \end{aligned} \quad (\text{A14})$$

where

$$n_k^{\text{samp}} = n_k(\beta_t) \exp\left[-\lambda - \mu(\beta_t)\beta_t + \frac{\hbar^2 k^2 \beta_t}{2m}\right], \quad (\text{A15})$$

and the preweight  $\Omega_0 \equiv \Omega(0)$  now depends on the set of particular values of  $\tilde{\alpha}_k$  at  $\beta=0$  obtained for a given sample, according to

$$\ln \Omega_0 = \sum_k |\tilde{\alpha}_k|^2 \left( \frac{1}{n_k^{\text{samp}}} - \frac{1}{\bar{n}_x} \right). \quad (\text{A16})$$

For most of the simulations reported here, taking  $n_k(\beta_t)$  to be just the ideal gas Bose-Einstein distribution  $n_k^{\text{id}}(\beta_t)$  was sufficient. However, once the chemical potential  $\mu(\beta_t)$  approaches or exceeds zero, this estimate is no longer useful. A better choice for  $n_k(\beta_t)$  is the density of states function  $\rho_k$  of the exact Yang and Yang solution [7], although it should be noted that this is not the density of actual particles that we seek. In practice, our approach was to first run a calculation based on this estimate  $n_k(\beta_t) = \rho_k(\beta_t)$ , obtain a better estimate of the real density from this full stochastic calculation by evaluating the expectation value of  $\hat{\Psi}_k^\dagger \hat{\Psi}_k$  using Eq. (22), then finally use this expectation value to choose an improved preweighting function  $n_k(\beta_t)$  for a ‘‘second-generation’’ calculation.

One important point to make regarding the choice of  $n_k(\beta_t)$  is that one should endeavor always to choose the preweighting guide density  $n_k(\beta_t)$  equal or greater than the real density, never smaller. The reasoning behind this is as follows: suppose first one chooses a  $n_k(\beta_t)$  guiding function that is much smaller than the true  $k$ -space density  $n_k^{\text{true}}(\beta_t)$ . This means that the variance of the  $\tilde{\alpha}_k$  samples will be too small to recover the physical value of the density upon averaging  $\langle |\tilde{\alpha}_k|^2 \Omega \rangle_S$  without resorting to very large weights for the largest  $|\tilde{\alpha}_k|$  samples. In practice, if the ratio  $n_k/n_k^{\text{true}}$  is small, then the typical trade-off that occurs is that the largest contribution to  $\Omega |\tilde{\alpha}_k|^2$  comes from those  $|\tilde{\alpha}_k|$  that are many standard deviations from the mean. Their rarity is compensated for by a very large  $\Omega$ . However, this is fatal for practical numbers of samples because, in fact, not even one of the samples one obtains ends up in this highest-contribution region at many standard deviations from the mean. For  $n_k/n_k^{\text{true}} \lesssim 1/2$ , the number of samples with  $|\tilde{\alpha}_k|^2 \geq n_k$  will be  $\propto S \Pi_k \exp[-(n_k^{\text{true}}/n_k)^2/2]$ , i.e., vanishing, leading to a systematic error.

In contrast, the opposite situation when  $n_k(\beta_t)$  is chosen too large is much more benign. Following the above reasoning, one gets a distribution of  $\tilde{\alpha}_k$  samples that is too broad, with the result that a majority of samples are too far away from physical values of  $|\tilde{\alpha}_k|^2$  and their excessive abundance must be compensated for by giving them a correspondingly small weight. However, for reasonably large numbers of trajectories, there always remains a core of the smallest samples that are in the region of most important contributions. The number of these samples is of the order of  $S \Pi_k n_k^{\text{true}}/n_k(\beta_t)$ , which is reasonable in practice as long as the estimate  $n_k(\beta_t)$  is not extremely poor.

Finally, it should be mentioned that superior importance sampling schemes to the crude one we have employed here could be implemented and may allow one to reach much lower temperatures than presented here. A first step would be to keep the  $\beta = \beta_t$  distribution estimate [Eq. (A13)] but estimate the resulting initial samples at  $\beta=0$  in a more accurate manner. To do this, one could choose the  $\beta = \beta_t$  samples according to  $\tilde{\alpha}_k^{(v)}(\beta_t) = \sqrt{n_k(\beta_t)} \eta_k$  and  $\ln \Omega(\beta_t) = 0$  as usual but then evolve them back in time to  $\beta=0$  numerically, using the deterministic part of the full equations [Eq. (21)]. This would give a superior estimate of the initial distribution as it takes into account  $g \neq 0$  mean field effects as well as kinetic evolution. Having these  $\beta=0$  samples, one would then proceed forward in time with the full stochastic evolution.



A further refinement would be to choose initial  $\beta=0$  samples via the Metropolis algorithm, so that the initial samples  $\vec{v}$  are distributed according to  $\mathcal{F}[\vec{v}]$ , where  $\mathcal{F}=[\Omega(\beta_i)]$  when  $\Omega(\beta_i)$  is calculated according to the deterministic part of the evolution [Eq. (21)], starting from  $\Omega(0)=0$ . This avoids the arbitrariness of the crude Gaussian choice [Eq. (A13)]. A final but numerically intensive approach would be to sample the phase-space variables  $\alpha_j(\beta_i)$  and  $\text{Im}[\ln \Omega](\beta_i)$  directly via a Monte Carlo Metropolis algorithm whose free parameters to be varied include both the initial noises  $\eta_k$  and all the time-dependent noises  $\xi_j^{(v)}(\beta)$  for a given time lattice  $\beta \in (0, \beta_i)$ .

#### 4. Trust indicators for sampling

One should mention two heuristic trust indicators that we use extensively to exclude bad sampling of the underlying phase-space distribution.

First, let us point out that the behavior of the evolution equation(2) is such that one builds up an approximately Gaussian distribution of the logarithmic variables (leaving aside the evolution of  $N_j$  itself, which is initially small). This means that the stochastic averages to be evaluated, e.g., in Eq. (25), involve means of *exponentials* of approximately Gaussian random variables (as per  $\bar{m}=\langle e^v \rangle$  with  $v$  Gaussian). A feature of such means is that if the variance of the *logarithm*  $\text{Re}[v]$  exceeds a value of around 10 the mean  $\bar{m}$  begins to have systematic error when calculated with any practical sample sizes. This is discussed in detail in [50,69]. As a result, when calculating observables with some expression  $\langle F(\vec{v}) \rangle_S$ , one must also check that the variance of its logarithm is small enough, i.e., that

$$\mathcal{V}_F = \langle [\ln|F(\vec{v})|]^2 \rangle_S - \langle \ln|F(\vec{v})| \rangle_S^2 \lesssim 10. \quad (\text{A17})$$

If this is not satisfied, the results for  $\langle F(\vec{v}) \rangle_S$  must be considered suspect.

Second, sampling problems of this sort usually make themselves visible if one compares two calculations with widely different sample sizes. In practice one can evaluate an average and its uncertainty with  $\mathcal{S}$  samples and with  $\mathcal{S}/10$  samples (where, of course,  $\mathcal{S}/10 \gg 1$ ). If the difference is statistically significant the result of the  $\mathcal{S}$  sample average again should be considered suspect.

#### 5. Choice of intermediate $\mu(\beta)$

If one is primarily interested in the behavior of the system around some target temperature  $\beta_t$  and chemical potential  $\mu(\beta_i)$  (alternatively, density), then the values of  $\mu(\beta)$  at intermediate times  $\beta < \beta_i$  can, in principle, be chosen at will.

In practice, however, some choices lead to smaller statistical uncertainty than others because the intermediate values of density affect the amount of noise generated during the evolution. A preliminary investigation of  $\mu$  choice in [50] indicated some heuristic guidelines that were also followed in the present work:

(i) It is advantageous to not vary  $\mu_e(\beta)$  too much over the course of the simulation. Excessive variation leads to increased noise.

(ii) A constant or piecewise-constant value of  $\mu_e$  is also advantageous because the ideal-gas part of the evolution can then be calculated exactly in logarithmic variables [Eq. (A7)], and step size is only important for the interaction part of the evolution.

(iii) It is advantageous to choose an initial density that is much smaller than the final one at  $\beta_i$  both for statistical sampling reasons and because this puts the initial gas much further into the classical decoherent regime ( $\tau \gg \gamma^2$ ), where the initial condition (12) applies than the final regime.

In practice, our simulations used the following form:

$$\mu_e(\beta) = \frac{1}{\Delta\beta} \ln \frac{z(\beta + \Delta\beta)}{z(\beta)}, \quad (\text{A18})$$

which is piecewise constant over a time step  $\Delta\beta$ , with the fugacity

$$z(\beta) = e^{\mu\beta} = \begin{cases} z_i & \text{when } \beta \leq \beta_i \\ z_t \exp\left[-\frac{\beta_t - \beta}{\beta_t - \beta_i} \ln \frac{z_t}{z_i}\right] & \text{when } \beta > \beta_i. \end{cases} \quad (\text{A19})$$

Here,  $\beta_t$  and  $z_t = e^{\mu\beta_t}$  are the target inverse temperature and fugacity and  $\beta_i$  and  $z_i$  are numerical constants for the initial high-temperature state that we chose to be  $z_i^2 = z_t^2/1000$  and  $\beta_i = \beta_t/1000$ .

Given the difficulty of precisely analyzing the statistical behavior, it is unclear whether a wiser choice of  $\mu(\beta)$  may lead to significant improvements over the results presented here. However, this is the most successful choice of those we tried.

#### APPENDIX B: INTEGRALS IN PERTURBATION THEORY IN $\gamma$

We begin with Eq. (32) and substitute the expression for  $\Gamma(k, \sigma)$  in Eq. (37) to give

$$\Delta g^{(2)}(r) = -\frac{g}{\hbar} \sqrt{\frac{m\beta}{\pi}} \int_0^\beta d\sigma \frac{\exp\left\{-\frac{r^2 m\beta}{4\hbar^2[\beta^2/4 - (\sigma - \beta/2)^2]}\right\}}{\sqrt{\beta^2/4 - (\sigma - \beta/2)^2}}. \quad (\text{B1})$$

Next we make the substitution  $t = (2/\beta)(\sigma - \beta/2)$  and  $y = r\sqrt{m/(\hbar^2\beta)}$  to give

$$\Delta g^{(2)}(r) = -\frac{g}{\hbar} \sqrt{\frac{m\beta}{\pi}} \int_{-1}^1 dt \frac{e^{-y^2/(1-t^2)}}{\sqrt{1-t^2}} \quad (\text{B2})$$

$$= -\frac{g}{\hbar} \sqrt{\frac{m\beta}{\pi}} e^{-y^2} \int_{-\infty}^{\infty} dx \frac{e^{-y^2 x^2}}{1+x^2}, \quad (\text{B3})$$

where the last equality follows from the substitution  $t = x/\sqrt{1+x^2}$ . The exponent in the integrand of Eq. (B3) can be represented as a Gaussian integral,



$$e^{-y^2x^2} = \frac{1}{\sqrt{\pi}} \int_{-\infty}^{\infty} dk e^{-k^2+2iky x}. \quad (\text{B4})$$

Then, changing the order of integration in Eq. (B3) we arrive at

$$\begin{aligned} \Delta g^{(2)}(r) &= -\frac{g}{\hbar\pi} \sqrt{m\beta} e^{-y^2} \int_{-\infty}^{\infty} e^{-k^2} \int_{-\infty}^{\infty} \frac{e^{i2kyx}}{1+x^2} dx dk \\ &= -\frac{2g\sqrt{m\beta}}{\hbar} \int_0^{\infty} e^{-(k+|y|)^2} dk. \end{aligned} \quad (\text{B5})$$

The final result shown in Eq. (38) follows trivially from a shift in the integration variable  $k \rightarrow k - |y|$  and the definition of the complimentary error function,

$$\text{erfc}(|y|) \equiv \frac{2}{\sqrt{\pi}} \int_{|y|}^{\infty} dk e^{-k^2}. \quad (\text{B6})$$

### APPENDIX C: INTEGRALS IN THE BOGOLIUBOV TREATMENT

We first evaluate the vacuum contribution  $G_0(r)$  [Eq. (54)]. Writing down the integral explicitly, in terms of  $k$  and transforming to another variable  $x = k\xi/2$ , we have

$$G_0(r) = \frac{2}{\pi\xi n} \int_0^{\infty} dk \left[ \frac{x}{\sqrt{1+x^2}} - 1 \right] \cos(2rx/\xi). \quad (\text{C1})$$

Integrating by parts gives

$$G_0(r) = -\frac{1}{\pi nr} \int_0^{\infty} dx \frac{\sin(2\sqrt{\gamma}rx)}{(1+x^2)^{3/2}}. \quad (\text{C2})$$

The integral in Eq. (C2) can be expressed in terms of special functions [70], giving

$$G_0(r) = -\sqrt{\gamma} [\mathbf{L}_{-1}(2\sqrt{\gamma}nr) - I_1(2\sqrt{\gamma}nr)]. \quad (\text{C3})$$

The finite temperature term  $G_T(r)$  [Eq. (57)] is evaluated by performing variable changes according to  $E = \hbar^2 k^2 / (2m)$ , followed by  $\epsilon = \sqrt{E(E+gn)}$ , and then  $x = \epsilon/gn$ . In this way we transform the integral over  $k$  to an integral over  $x$ ,

$$G_T(r) = \sqrt{\frac{2mg}{\pi^2 \hbar^2 n}} \int_0^{\infty} dx \left[ \frac{\sqrt{1+x^2}-1}{1+x^2} \right]^{1/2} \frac{\cos[k(x)r]}{e^{gnx/T}-1}, \quad (\text{C4})$$

where  $k(x) = [2mgn(\sqrt{1+x^2}-1)/\hbar^2]^{1/2}$ . So far we have not made any additional assumptions or approximations.

By inspecting the integrand in Eq. (C4) one can see that for  $T \ll gn$  the main contribution to the integral comes from  $x \ll 1$ . Therefore for  $T \ll gn$  ( $\tau \ll \gamma$ ) we can simplify the integral by treating  $x$  in the integrand as a small parameter. Accordingly, we obtain

$$\left[ \frac{\sqrt{1+x^2}-1}{1+x^2} \right]^{1/2} \approx \frac{1}{\sqrt{2}} x, \quad x \ll 1, \quad (\text{C5})$$

$$k(x) \approx \sqrt{\frac{mgn}{\hbar^2}} x, \quad x \ll 1, \quad (\text{C6})$$

and therefore

$$G_T(r) \approx \frac{\tau^2}{4\pi\gamma^{3/2}} \int_0^{\infty} dy \frac{y \cos(\pi r y / 2\sqrt{\gamma})}{e^y - 1}, \quad (\text{C7})$$

where we have introduced  $y = gn x / T = \epsilon / T$ . Finally we make use of the following integral:

$$\int_0^{\infty} dy \frac{y \cos(ay)}{e^y - 1} = \frac{1}{2a} - \frac{\pi^2}{2} \text{cosech}^2(\pi a) \quad (\text{C8})$$

and obtain Eq. (58).

In the opposite limit, dominated by thermal fluctuations and corresponding to  $\gamma \ll \tau \ll 1$ , we first note that large thermal fluctuations correspond to  $\tilde{n}_k \gg 1$ , which in turn requires  $\epsilon_k / T \ll 1$ . Thus, we replace  $\tilde{n}_k$  in integral (55) by  $\tilde{n}_k = [\exp(\epsilon_k/T) - 1]^{-1} \approx T / \epsilon_k \gg 1$ . As a result, the thermal contribution  $G_T(r)$  becomes

$$\begin{aligned} G_T(r) &\approx \frac{1}{\pi n} \int_{-\infty}^{+\infty} dk \frac{E_k T}{\epsilon_k} \cos(kr) \\ &= \frac{4mT}{\pi \hbar^2 n} \int_0^{+\infty} dk \frac{\cos(kr)}{k^2 + (2/\xi)^2} \\ &= \frac{mT\xi}{\hbar^2 n} e^{-2r/\xi}, \end{aligned} \quad (\text{C9})$$

which is valid for  $r/\xi \ll 1$ . Rewriting this in terms of the dimensionless parameters  $\gamma$  and  $\tau$  we obtain Eq. (61). For  $r/\xi \gg 1$  the cosine term becomes important and the values of momenta in the integral equation (C4) are cut off by  $1/r \ll \xi$ . In this regime one can use the approximation that led to Eq. (C8).

### APPENDIX D: INTEGRALS IN PERTURBATION THEORY IN $1/\gamma$

We begin by evaluating the direct contribution given by Eq. (63) by substituting Eq. (67),

$$\begin{aligned} \Delta g_d^{(2)} &= \int_0^{\beta} d\sigma \int_{-\infty}^{\infty} \frac{dk}{2\pi} \left( -\frac{2\hbar^2 k^2}{mn\gamma} \right) e^{ikr - \sigma \hbar^2 k^2 (\beta - \sigma) / m\beta} \\ &= \frac{-1}{\pi\gamma} \sqrt{\frac{\tau}{2}} \int_0^1 ds \int_{-\infty}^{\infty} dq q^2 e^{iqy - sq^2(1-s)}, \end{aligned} \quad (\text{D1})$$

where we have affected the change of variables  $\sigma = \beta s$ ,  $q = \sqrt{\beta \hbar^2 / mk}$ , and  $y = \sqrt{m / (\beta \hbar^2)} r = \sqrt{(\pi^2 / 2)} r$ . The integration with respect to  $q$  can then be done using integration by parts, which yields

$$\begin{aligned} \Delta g_d^{(2)} &= \frac{-1}{4\gamma} \sqrt{\frac{\tau}{2\pi}} \int_0^1 ds \frac{2s(1-s) - y^2}{s^{5/2}(1-s)^{5/2}} e^{-y^2/[4s(1-s)]} \\ &= \frac{-1}{\gamma} \sqrt{\frac{2\tau}{\pi}} \int_{-1}^1 dt \left( 1 - \frac{2y^2}{1-t^2} \right) \frac{e^{-y^2/(1-t^2)}}{(1-t^2)^{3/2}}, \end{aligned} \quad (\text{D2})$$

where the last equality follows from the substitution

$s=(t+1)/2$ . The simplest way to solve the integral in Eq. (D2) is by comparison with Eq. (B2) in Appendix B. In doing so, one may observe

$$\int_{-1}^1 dt \left(1 - \frac{2y^2}{1-t^2}\right) \frac{\exp\left[-\frac{y^2}{1-t^2}\right]}{(1-t^2)^{3/2}} \quad (\text{D3})$$

$$= \frac{d^2}{dy^2} \int_{-1}^1 dt \frac{\exp\left[-\frac{y^2}{1-t^2}\right]}{\sqrt{1-t^2}} = \pi \frac{d^2}{dy^2} \text{erfc}(|y|). \quad (\text{D4})$$

The result shown in Eq. (68) then follows trivially from this.

In order to calculate the exchange contribution we begin with Eq. (64) and substitute Eq. (67), which immediately yields

$$\Delta g_e^{(2)}(r) = \frac{1}{\gamma} \sqrt{\frac{\pi\tau}{2}} e^{-in\pi^2/2} F_e(\sqrt{\pi^2 r^2/2}), \quad (\text{D5})$$

where  $F_e(y) = \int_0^1 ds \int dq q^2 e^{-s(1-s)q^2 + i(1-2s)qy} / \pi^{3/2}$  and  $s$ ,  $q$ , and  $y$  are defined the same as was for the direct contribution. The integration with respect to  $q$  can be carried out using inte-

gration by parts, leaving an integral with respect to  $s$ ,

$$\begin{aligned} & \int_0^1 ds \frac{\exp\left[-\frac{y^2(1-2s)^2}{4s(1-s)}\right]}{s^{3/2}(1-s)^{3/2}} \left[1 - \frac{y^2(1-2s)^2}{2s(1-s)}\right] \\ &= 4 \int_{-1}^1 dv \frac{\exp\left[-\frac{y^2 v^2}{1-v^2}\right]}{(1-v^2)^{3/2}} \left[1 - \frac{2v^2 y^2}{1-v^2}\right] \\ &= 4 \int_{-\infty}^{\infty} dt [1 - 2y^2 t^2] e^{-y^2 t^2}, \end{aligned} \quad (\text{D6})$$

where the first equality comes from the substitution  $s=(v+1)/2$  and the second from  $v=t/\sqrt{1+t^2}$ . Both terms are standard definite integrals; it is straightforward to show that

$$\Delta g_e^{(2)} = \frac{4}{n\gamma} \delta(r). \quad (\text{D7})$$

Thus the only effect of the exchange contribution is to cancel the delta-function contribution coming from the direct contribution at  $r=0$ .

- 
- [1] R. Hanbury Brown and R. Q. Twiss, *Nature (London)* **177**, 27 (1956).
- [2] M. Yasuda and F. Shimizu, *Phys. Rev. Lett.* **77**, 3090 (1996).
- [3] M. Schellekens, R. Hoppeler, A. Perrin, J. Viana Gomes, D. Boiron, and C. I. Westbrook, *Science* **310**, 648 (2005).
- [4] T. Jelts, J. M. McNamara, W. Hogervorst, W. Vassen, V. Krachmalnicoff, M. Schellekens, A. Perrin, H. Chang, D. Boiron, A. Aspect, and C. I. Westbrook, *Nature (London)* **445**, 402 (2007).
- [5] E. H. Lieb and W. Liniger, *Phys. Rev.* **130**, 1605 (1963).
- [6] E. H. Lieb, *Phys. Rev.* **130**, 1616 (1963).
- [7] C. N. Yang and C. P. Yang, *J. Math. Phys.* **10**, 1115 (1969).
- [8] V. E. Korepin, N. M. Bogoliubov, and A. G. Izergin, *Quantum Inverse Scattering Method and Correlation Functions* (Cambridge University Press, Cambridge, 1993).
- [9] T. Giamarchi, *Quantum Physics in One Dimension* (Oxford University Press, New York, 2004).
- [10] A. O. Gogolin, A. A. Nersisyan, and A. M. Tsvelik, *Bosonization and Strongly Correlated Systems* (Cambridge University Press, Cambridge, 2004).
- [11] M. D. Girardeau, *J. Math. Phys.* **1**, 516 (1960); M. D. Girardeau, *Phys. Rev.* **139**, B500 (1965); see also L. Tonks, *ibid.* **50**, 955 (1936).
- [12] A. Görlitz, J. M. Vogels, A. E. Leanhardt, C. Raman, T. L. Gustavson, J. R. Abo-Shaer, A. P. Chikkatur, S. Gupta, S. Inouye, T. Rosenband, and W. Ketterle, *Phys. Rev. Lett.* **87**, 130402 (2001).
- [13] F. Schreck, L. Khaykovich, K. L. Corwin, G. Ferrari, T. Bourdel, J. Cubizolles, and C. Salomon, *Phys. Rev. Lett.* **87**, 080403 (2001).
- [14] M. Greiner, I. Bloch, O. Mandel, T. W. Hänsch, and T. Esslinger, *Phys. Rev. Lett.* **87**, 160405 (2001).
- [15] M. Greiner, I. Bloch, O. Mandel, T. W. Hänsch, and T. Esslinger, *Appl. Phys. B: Lasers Opt.* **73**, 769 (2001).
- [16] S. Richard, F. Gerbier, J. H. Thywissen, M. Hugbart, P. Bouyer, and A. Aspect, *Phys. Rev. Lett.* **91**, 010405 (2003).
- [17] H. Moritz, T. Stöferle, M. Kohl, and T. Esslinger, *Phys. Rev. Lett.* **91**, 250402 (2003).
- [18] B. Laburthe Tolra, K. M. O'Hara, J. H. Huckans, W. D. Phillips, S. L. Rolston, and J. V. Porto, *Phys. Rev. Lett.* **92**, 190401 (2004).
- [19] B. Paredes, A. Widera, V. Murg, O. Mandel, S. Fölling, I. Cirac, G. V. Shlyapnikov, T. Hänsch, and I. Bloch, *Nature (London)* **429**, 277 (2004).
- [20] T. Kinoshita, T. Wenger, and D. S. Weiss, *Science* **305**, 1125 (2004).
- [21] T. Kinoshita, T. Wenger, and D. S. Weiss, *Phys. Rev. Lett.* **95**, 190406 (2005).
- [22] T. Stöferle, H. Moritz, C. Schori, M. Kohl, and T. Esslinger, *Phys. Rev. Lett.* **92**, 130403 (2004).
- [23] T. P. Meyrath, F. Schreck, J. L. Hanssen, C. S. Chuu, and M. G. Raizen, *Phys. Rev. A* **71**, 041604(R) (2005).
- [24] J. Esteve, J. B. Trebbia, T. Schumm, A. Aspect, C. I. Westbrook, and I. Bouchoule, *Phys. Rev. Lett.* **96**, 130403 (2006).
- [25] S. Hofferberth, I. Lesanovsky, B. Fischer, T. Schumm, and J. Schmiedmayer, *Nature (London)* **449**, 324 (2007).
- [26] A. H. van Amerongen, J. J. P. van Es, P. Wicke, K. V. Kheruntsyan, and N. J. van Druten, *Phys. Rev. Lett.* **100**, 090402 (2008).
- [27] Y. Castin, R. Dum, E. Mandonnet, A. Minguzzi, and I. Carusotto, *J. Mod. Opt.* **47**, 2671 (2000).
- [28] D. M. Gangardt and G. V. Shlyapnikov, *Phys. Rev. Lett.* **90**, 010401 (2003).
- [29] D. M. Gangardt and G. V. Shlyapnikov, *New J. Phys.* **5**, 79

- (2003).
- [30] K. V. Kheruntsyan, D. M. Gangardt, P. D. Drummond, and G. V. Shlyapnikov, *Phys. Rev. Lett.* **91**, 040403 (2003).
- [31] M. A. Cazalilla, *Phys. Rev. A* **67**, 053606 (2003); *New J. Phys.* **37**, S1 (2004).
- [32] K. V. Kheruntsyan, D. M. Gangardt, P. D. Drummond, and G. V. Shlyapnikov, *Phys. Rev. A* **71**, 053615 (2005).
- [33] G. E. Astrakharchik and S. Giorgini, *Phys. Rev. A* **68**, 031602(R) (2003); *J. Phys. B* **39**, S1 (2006).
- [34] P. D. Drummond, P. Deuar, and K. V. Kheruntsyan, *Phys. Rev. Lett.* **92**, 040405 (2004).
- [35] A. Lenard, *J. Math. Phys.* **5**, 930 (1964).
- [36] T. D. Schultz, *J. Math. Phys.* **4**, 666 (1963).
- [37] J.-S. Caux and P. Calabrese, *Phys. Rev. A* **74**, 031605(R) (2006).
- [38] J.-S. Caux, P. Calabrese, and N. A. Slavnov, *J. Stat. Mech.: Theory Exp.* (2007) 01008.
- [39] J. Brand and A. Yu. Cherny, *Phys. Rev. A* **72**, 033619 (2005).
- [40] M. Khodas, M. Pustilnik, A. Kamenev, and L. I. Glazman, *Phys. Rev. Lett.* **99**, 110405 (2007).
- [41] A. Imambekov and L. I. Glazman, *Phys. Rev. Lett.* **100**, 206805 (2008).
- [42] A. Yu. Cherny and J. Brand, *Phys. Rev. A* **73**, 023612 (2006).
- [43] E. H. Lieb, R. Seiringer, J. P. Solovej, and J. Yngvason, e-print arXiv:cond-mat/0610117.
- [44] D. S. Petrov, D. M. Gangardt, and G. V. Shlyapnikov, *J. Phys. IV* **116**, 3 (2004).
- [45] Y. Castin, *J. Phys. IV* **116**, 89 (2004).
- [46] A. G. Sykes, D. M. Gangardt, M. J. Davis, K. Viering, M. G. Raizen, and K. V. Kheruntsyan, *Phys. Rev. Lett.* **100**, 160406 (2008).
- [47] P. Deuar and P. D. Drummond, *Phys. Rev. A* **66**, 033812 (2002).
- [48] P. D. Drummond and P. Deuar, *J. Opt. B: Quantum Semiclassical Opt.* **5**, S281 (2003).
- [49] P. Deuar and P. D. Drummond, *J. Phys. A* **39**, 2723 (2006).
- [50] P. Deuar, Ph.D. thesis, The University of Queensland, 2005, eprint arXiv:cond-mat/0507023.
- [51] T. C. Li, H. Kelkar, D. Medellin, and M. G. Raizen, *Opt. Express* **16**, 5465 (2008).
- [52] M. Olshanii, *Phys. Rev. Lett.* **81**, 938 (1998).
- [53] I. Bouchoule, K. V. Kheruntsyan, and G. V. Shlyapnikov, *Phys. Rev. A* **75**, 031606(R) (2007).
- [54] A. G. Sykes, P. D. Drummond, and M. J. Davis, *Phys. Rev. A* **76**, 063620 (2007).
- [55] P. D. Drummond and C. W. Gardiner, *J. Phys. A* **13**, 2353 (1980).
- [56] C. W. Gardiner, *Quantum Noise* (Springer-Verlag, Berlin, 1992).
- [57] A. Gilchrist, C. W. Gardiner, and P. D. Drummond, *Phys. Rev. A* **55**, 3014 (1997).
- [58] Note that Eq. (30) only contains four terms coming from Wick's theorem; the other 20 terms are disconnected corrections (in the language of Feynman diagrams) and hence only produce corrections to the single particle Green's functions. That is they represent the interacting corrections to the relation between chemical potential and density.
- [59] M. Naraschewski and R. J. Glauber, *Phys. Rev. A* **59**, 4595 (1999).
- [60] N. D. Mermin and H. Wagner, *Phys. Rev. Lett.* **17**, 1133 (1966); P. C. Hohenberg, *Phys. Rev.* **158**, 383 (1967).
- [61] D. S. Petrov, G. V. Shlyapnikov, and J. T. M. Walraven, *Phys. Rev. Lett.* **85**, 3745 (2000).
- [62] T. Cheon and T. Shigehara, *Phys. Rev. Lett.* **82**, 2536 (1999); D. Sen, *J. Phys. A* **36**, 7517 (2003).
- [63] J. Friedel, *Nuovo Cimento, Suppl.* **7**, 287 (1958).
- [64] G. E. Astrakharchik, J. Boronat, J. Casulleras, and S. Giorgini, *Phys. Rev. Lett.* **95**, 190407 (2005); M. Batchelor, M. Bortz, X. W. Guan, and N. Oelkers, *J. Stat. Mech.: Theory Exp.* (2005), L10001.
- [65] J. F. Corney and P. D. Drummond, *Phys. Rev. Lett.* **93**, 260401 (2004).
- [66] T. Aimi and M. Imada, *J. Phys. Soc. Jpn.* **76**, 084709 (2007); **76**, 113708 (2007).
- [67] I. Carusotto and Y. Castin, *J. Phys. B* **34**, 4589 (2001).
- [68] P. D. Drummond and I. K. Mortimer, *J. Comput. Phys.* **93**, 144 (1991).
- [69] P. Deuar and P. D. Drummond, *J. Phys. A* **39**, 1163 (2006).
- [70] *Handbook of Mathematical Functions*, edited by M. Abramowitz and I. A. Stegun (Dover, New York, 1965).